GERMAN - MONGOLIAN INSTITUTE FOR RESOURCES AND TECHNOLOGY

The present work was submitted to

The German-Mongolian Institute for Resources and Technology

INVESTIGATION OF INERT ANODES FOR NEODYMIUM ELECTROWINNING: CORROSION OF NICKEL FERRITE-BASED ANODES BY NdF_3-LiF MELT

Bachelor's Thesis

By

Zolzaya Purevjav

Study program: Raw Materials and Process Engineering

Student ID: B2100627

1st Supervisor/Examiner: Prof. Dr. – Ing. Bayanmunkh Myagmarsuren

2nd Supervisor/Examiner: Prof. Dr. – Ing. Alexandros Charitos

Advisor: M.Sc. Ulziikhuu Otgonbayar

Ulaanbaatar/Nalaikh

2025

GERMAN - MONGOLIAN INSTITUTE FOR RESOURCES AND TECHNOLOGY

The present work was submitted to

the German-Mongolian Institute for Resources and Technology

INVESTIGATION OF INERT ANODES FOR NEODYMIUM ELECTROWINNING: CORROSION OF NICKEL FERRITE-BASED ANODES BY NdF_3-LiF MELT

Bachelor's Thesis

By

Zolzaya Purevjav

Study program: Raw Materials and Process Engineering

Student ID: B2100627

1st Supervisor/Examiner: Prof. Dr. – Ing. Bayanmunkh Myagmarsuren

2nd Supervisor/Examiner: Prof. Dr. – Ing. Alexandros Charitos

Advisor: M.Sc. Ulziikhuu Otgonbayar

Ulaanbaatar/Nalaikh

2025

Statutory Declaration

Purevjav, Zolzaya	B2100627
Last Name, First Name	Student ID Number

I hereby affirm in lieu of an oath that I provided the submitted bachelor thesis

INVESTIGATION OF INERT ANODES FOR NEODYMIUM ELECTROWINNING: CORROSION OF NICKEL FERRITE-BASED ANODES BY NdF_3-LiF MELT

I did not use any sources other than those stated. In case that the work is additionally submitted on a data medium, I declare that the written and the electronic form are completely identical. The work was not submitted in the same or similar form to any examination authority.

Nalaikh, 28.05.2025	
Place, Date	Signature

Acknowledgements

First and foremost, I would like to express my sincere gratitude to Prof. Alexandros Charitos for accepting my bachelor's thesis experimental work at TU Bergakademie Freiberg and for his invaluable supervision. I am truly honored by his acceptance as my supervisor.

I am deeply grateful to M.Sc. Ulziikhuu Otgonbayar for her unwavering guidance, support, and supervision. This work would not have been possible without her insightful advice and continuous assistance. Her willingness to share her knowledge, engage in discussions, and provide help throughout my research has been truly invaluable.

My sincere appreciation also goes to Prof. Bayanmunkh Myagmarsuren for his supervision and support. I am equally honored and grateful for his acceptance as my supervisor.

I would like to extend my heartfelt thanks to all the members, staff, and research assistants of the Institute of Nonferrous Metallurgy and Purest Materials (INEMET) for their assistance and support during my work.

Finally, I am deeply grateful to my family and friends for their unwavering encouragement and support.

This work would not have been possible without all of you.

Table of content

1. Introduction

Neodymium (Nd) is a rare earth element (REE) not found in nature in its pure metallic form. Although it is classified as a rare earth element, it is not rare. Its abundance in the Earth's crust is approximately 30 ppm, making it the 60th most abundant element [1].
As technology advances, the importance of Nd increases due to its high magnetic strength (strong magnetic field generation), good electrical conductivity, and lightweight yet high mechanical strength [2]. Its major industrial use is in the production of neodymium-iron-boron (NdFeB) magnets, which are among the most powerful permanent magnets. These magnets are widely used in electric motors, wind turbine generators, hard disk drives, headphones, and various other high-tech applications [3]
High-purity Nd is required to use Nd for these applications. Therefore, the final step for Nd production is molten salt electrolysis. At high temperatures (around 1050°C), neodymium oxide is dissolved in NdF_3-LiF electrolyte. An oxidation reaction occurs at the anode to supply electrons to the cathode, where neodymium ions are reduced to metallic neodymium. Conventionally, carbon is used as an anode where oxygen undergoes an oxidation reaction, furthermore, it reacts with the carbon anode to produce greenhouse gasses (GHGs): CO_2 and CO. At high voltage, the carbon anode reacts with fluorine-containing electrolyte and forms perfluorocarbons (PFC) gasses which are highly environmentally harmful GHGs [4, 5]. Due to the continuous consumption of the carbon anode in the cell and GHG emission, a new inert anode should be investigated.
To become an ideal inert anode, it should fulfill some requirements, which are:

- Economically feasible
- Low corrosion rate
- Low contamination in the produced pure metal
- Good electrical conductivity [6]

When selecting an inert anode for Nd molten salt electrolysis, these factors are taken into account, and the corrosion behavior of potential anode materials is studied.

This bachelor thesis aims to investigate the corrosion of nickel ferrite-based inert anodes in NdF_3-LiF melts to assess their suitability for Nd electrowinning.

To evaluate the corrosion resistance, an immersion test was conducted, which shows the maximum corrosion behavior of the anode by applying no current to the cell. The dissolution of the anode in the melt and the corrosion depth are measured to identify its corrosion behavior. Based on these findings, the nickel ferrite-based inert anode is tested in Nd molten salt electrolysis.

The results of this study will provide valuable insights into the feasibility of using nickel ferrite-based anodes as a corrosion-resistant alternative to traditional carbon anodes in Nd electrowinning.

2. State of art

2.1 Neodymium overview

2.1.1. Introduction to Neodymium

Nd is a rare earth element (REE) with atomic number 60, belonging to the lanthanide group. It is a silvery-white metal that oxidizes upon exposure to air. Despite being classified as a REE, Nd is relatively abundant in the Earth's crust, the 60th abundant element. It is primarily extracted from minerals called bastnasite and monazite, which contain a specific amount of REE. Nd beneficiation is a relatively recent and complex metallurgical process. The initial beneficiation steps involve physical separation techniques such as flotation, gravity separation, and magnetic separation, followed by chemical processes like acid leaching, solvent extraction [7, 8].

Important physical properties of Nd are listed in Table 1: Neodymium properties.

Table 1: Neodymium properties

Atomic number	60
Atomic mass	144.24g/mol
Density	7.01 g/cm^3
Melting point	1024°C
Boiling point	3074°C

Due to its strong metallic bonding, Nd exhibits high thermal and chemical stability at elevated temperatures. Its relatively high density, melting point, and boiling point contribute to its suitability in demanding processes such as metallurgy, electrowinning, and the production of high-performance permanent magnets. These properties ensure that Nd can maintain structural integrity and reactivity under harsh industrial conditions.

2.1.2. Importance and Applications

Nd is widely used in various high-tech applications due to its exceptional magnetic and optical properties:

- Neodymium-Iron-Boron (NdFeB) Magnets: Used in electric vehicle (EV) motors, wind turbines, hard disk drives, and high-performance motors.
- Optical and Laser Technologies: Found in Nd:YAG lasers for medical procedures, material processing, and fiber optic communication systems.
- Glass and Ceramics: Used for coloration in high-quality optics, sunglasses, and protective welding goggles.
- Metal Alloys: Strengthens steel and aluminum alloys in aerospace and structural applications.

2.1.3. Global Production and Market Trend

As shown in Figure 1, China accounts for 85% of global Nd production, and it remains the center of Nd research. Other notable producers include the United States, Australia, Myanmar, and Russia [9]. In parallel, the growing demand for electric vehicles and renewable energy technologies has led to an annual growth rate of 8–10% in Nd consumption. Price fluctuations between $50,000 and $250,000 per metric ton, and are influenced by supply chain constraints and geopolitical factors [10].

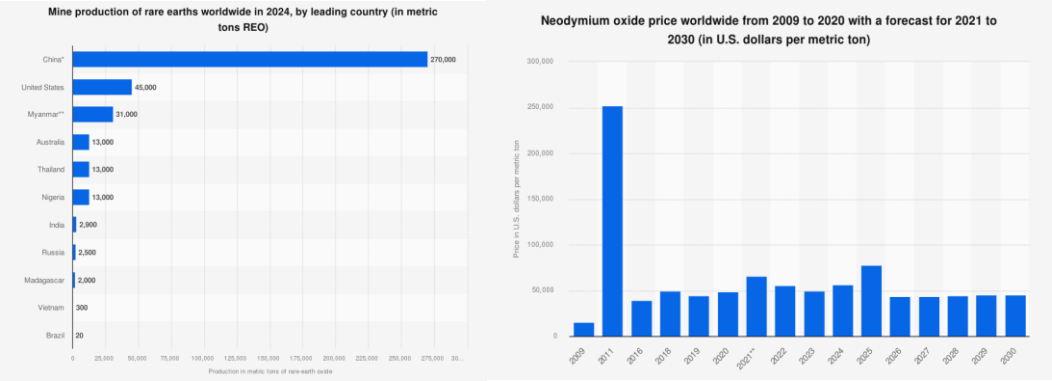

Figure 1: (a) Leading Countries in rare earth mine production in 2023 Global (data retrieved from [9]), (b) Neodymium oxide (REO) price forecast (2009–2030) (data retrieved from [10])

For comparison, copper is an essential industrial metal, which is right before Nd regarding its abundance, with prices around $9,600 per metric ton. This makes Nd roughly 8 times more expensive than copper, reflecting its specialized applications and limited availability.

2.2 Molten salt electrolysis

Electrolysis is the electrochemical process where a non-spontaneous reaction is driven by the applied voltage. When the electric current passes through the electrolyte, ions in the electrolyte migrate to respective electrodes, where the cation is reduced at the cathode (negative electrode), and the anion is oxidized at the anode (positive electrode).

Electrolysis can be classified into two main types: aqueous electrolysis and molten salt electrolysis.

- Aqueous electrolysis

  This method is used when the element being reduced or oxidized has a relatively higher electrochemical potential than water, allowing the reaction to take place in an aqueous solution, where water remains thermodynamically stable. However, this is generally true under standard ideal conditions. In practice, conditions can be adjusted to manipulate the overvoltage and allow the deposition of metals with lower redox potentials than hydrogen.

- Molten salt electrolysis

  In molten salt electrolysis, water is absent, and only metal cations and nonmetal anions from the molten salt participate in the electrochemical reactions. This method is particularly suitable for metals with reduction potentials relatively lower than that of water, as aqueous electrolysis becomes impractical under these conditions.

The electrochemical potential of a species refers to the potential energy that drives its movement during a redox process. The reduction potential of metals compared to hydrogen determines whether they can be reduced in an aqueous or molten salt system. Metals with higher reduction potentials than hydrogen ($E° > 0.00$ V) can be reduced in aqueous solutions, whereas those with lower reduction potentials ($E° < 0.00$ V) favor hydrogen evolution. Molten salt electrolysis is essential for extracting highly reactive metals like Al and Nd, which have highly negative reduction potentials.

Table 2: Standard reduction potential

Reduction reaction	Standard electrode potential (E°) (V)
$Ag^+ + e^- \rightarrow Ag$	0.8
$Fe^{3+} + e^- \rightarrow Fe^{2+}$	0.77
$Cu^{2+} + 2e^- \rightarrow Cu$	0.34
$2H^+ + 2e^- \rightarrow H_2$	0
$Ni^{2+} + 2e^- \rightarrow Ni$	-0.25
$Fe^{2+} + 2e^- \rightarrow Fe$	-0.44
$Zn^{2+} + 2e^- \rightarrow Zn$	-0.76
$Al^{3+} + 3e^- \rightarrow Al$	**-1.66**
$Mg^{2+} + 2e^- \rightarrow Mg$	-2.37
$Nd^{3+} + 3e^- \rightarrow Nd$	**-2.43**
$Ca^{2+} + 2e^- \rightarrow Ca$	-2.87
$Ba^{2+} + 2e^- \rightarrow Ba$	-2.9
$Li^+ + e^- \rightarrow Li$	-3.05

2.1.1 State of art - Aluminum molten salt electrolysis

In the Al production industry, the Hall-Héroult process is the final step of the Al purification process. Since Al has a significantly more negative reduction potential than hydrogen, aqueous electrolysis is unsuitable for the electrodeposition of Al.

Alumina (Al_2O_3) is produced from the Bayer process, where impurities are removed from bauxite. Since Al_2O_3 has a very high melting point (2072°C), it is dissolved in molten cryolite (typically Na_3AlF_6), which lowers the operating temperature to around 950-1000°C [11]. The electrolysis is conducted in a carbon-lined cell, where electrodes are also made of carbon, as shown in the simplified Hall-Héroult cell in Figure 2. The carbon cathode is located at the bottom of the cell, whereas the carbon anode is suspended in the molten electrolyte.

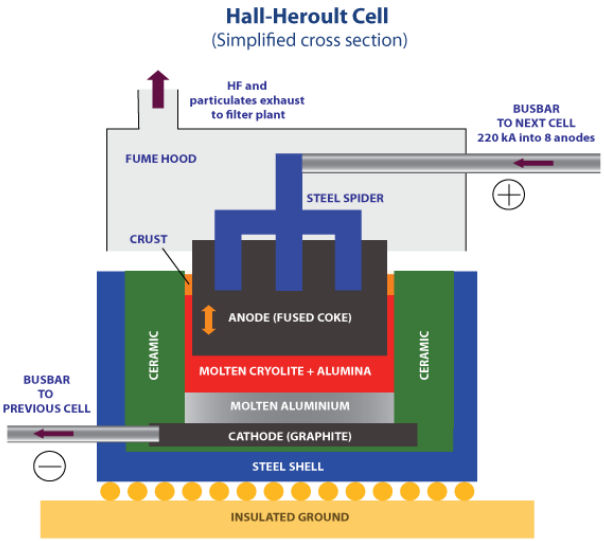

Figure 2: Hall-Héroult cell simplified (Source of the illustration [12])

The system's principle is that Al_2O_3 is reduced at the cathode, while oxide ions migrate to the anode and are released as oxygen gas. The corresponding reactions are shown in *Reaction (1)* and *Reaction (2)*. However, behind this process lies a more complex series of reactions. The Al_2O_3 dissolves into the electrolyte to form Al oxyfluorides, which then undergo oxidation at the anode.

$$\textit{Cathode: } Al^{3+} + 3e^- = Al \qquad (1)$$

$$\text{Anode: } 2O^{2-} = O_2 + 4e^- \qquad (2)$$

While the Hall-Héroult process produces aluminum with a purity of about 99.5%, it also generates significant carbon emissions (CO_2 and CO) due to the consumption of carbon anodes, raising environmental concerns.

$$C + O_2 = CO_2 \qquad (3)$$

$$C + \tfrac{1}{2} O_2 = CO \qquad (4)$$

Moreover, undesirable side reactions between the cryolite electrolyte and the carbon anode result in the formation of PFCs, such as CF_4 and C_2F_6, according to *Reaction (5)* and *(6)*, which are potent GHG contributing to global warming [13].

$$Na_3AlF_6 + \tfrac{3}{4} C = Al + \tfrac{3}{4} CF_4 + 3\,NaF \qquad (5)$$

$$Na_3AlF_6 + C = Al + \tfrac{1}{2} C_2F_6 + 3\,NaF \qquad (6)$$

According to Global Warming Potential (GWP) values, CF_4 has a GWP of approximately 6500, and C_2F_6 has a GWP of around 9200 over a 100-year time horizon, making them significantly more potent GHG than CO_2 [14].

In response to these concerns, there has been growing interest in developing inert anodes for Al electrolysis. Inert anodes significantly reduce harmful emissions by eliminating the consumption of carbon anodes, which are a major source of CO_2, CF_4 and C_2F_6. While carbon anodes are consumable and increasingly expensive in terms of raw materials and production infrastructure, the economic viability of inert anodes remains under evaluation. Challenges such as higher cell voltages and the loss of heat from C oxidation may increase operational costs. Nonetheless, inert anodes offer promising environmental advantages and the potential for long-term sustainability in the aluminum industry [15].

Proposed inert anode: Cermet anode

Cermet anodes, which combine a metal matrix with ceramic materials, have emerged as a viable solution. In terms of metallic properties, cermet material has good thermal and electrical conductivity, which allows accelerating the electrolysis process. On the other hand, cermet has good thermal resistance and a wide range of electrochemical stability. However, cermets also face challenges such as poor thermal shock resistance, brittleness, and potential degradation under fluctuating thermal or electrochemical conditions, which can limit their longevity and mechanical reliability during industrial operation [16].

$NiFe_2O_4$-based inert cermet anodes have been extensively investigated for Al molten salt electrolysis due to their favorable corrosion resistance and electrical properties. According to Olsen and Thonstad [17], in Al molten salt electrolysis, $NiFe_2O_4$-based inert cermet anodes were investigated in a NaF/AlF_3-based electrolyte with varying metallic phase additions (0%, 17%, and 23%). Among the metallic components, Ni exhibited significantly lower dissolution into the electrolyte compared to Cu and Fe, which was attributed to its lower mass transfer coefficient. Furthermore, due to the NiO activity being less than unity, the activity of Fe_3O_4 becomes relatively higher, potentially leading to an increased rate of Fe dissolution from the anode into the melt. The authors proposed that the corrosion of cermet anodes in cryolite-based melts is primarily governed by a mass transport-controlled mechanism [17] [18].

Further investigations revealed that under an argon atmosphere, the spinel phase dissolved, NiO was reduced, and metallic Ni accumulated at the anode surface. Notably, variations in cermet ratios or alumina content did not significantly influence degradation behavior, which followed a similar path in all tested cases [19] [20].

Corrosion behavior

Nickel ferrite ($NiFe_2O_4$) also exhibits notable electrical conductivity, but during electrolysis, Fe^{3+} ions in its structure are more susceptible to corrosion by the molten salt electrolyte. A proposed chemical corrosion reaction by He [21] is shown in *Reaction (7)*.

$$NiFe_2O_4 + 2AlF_3 \rightarrow NiO + 2FeF_3 + Al_2O_3 \quad (7)$$

In practice, $NiFe_2O_4$ demonstrates slight chemical solubility in cryolite melts; for instance, approximately 0.18% NiO was reported to dissolve in a melt containing 5 wt% Al_2O_3 and 0.003 wt% Fe_2O_3. Under electrochemical conditions, the anode may also undergo the following *Reaction (8),* according to He [21]:

$$2Al + NiFe_2O_4 \rightarrow NiAl_2O_4 + 2Fe \quad (8)$$

The development of inert anodes in Al electrolysis offers valuable insights for other high-temperature molten salt systems, including neodymium electrolysis, which presents its unique challenges.

2.1.2 Neodymium molten salt electrolysis

Electrowinning, or molten salt electrolysis, is the predominant industrial method for extracting rare earth metals from their oxides. In this process, only the oxide species dissolved in the molten salt undergoes electrochemical reduction, making the solubility of the oxide in the electrolyte a critical factor for process efficiency [22]. A typical electrowinning cell for Nd consists of a tungsten or molybdenum cathode and a carbon anode. The electrochemical reactions for Nd_2O_3 electrolysis proceed as follows Reaction (9)

$$\text{Cathode:} \quad 2Nd_2O_3 + 12e^- \rightarrow 4Nd + 6O^{2-} \quad (9)$$

$$\text{Anode:} \quad 3C + 6O^{2-} \rightarrow 3CO_2 + 12e^- \quad (10)$$

$$\text{Overall:} \quad 2Nd_2O_3 + 3C \rightarrow 4Nd + 3CO_2 \quad (11)$$

This process typically operates at cathodic current densities exceeding 1 A cm^{-2} and a cell voltage of around 3.6 V. The dominant overpotentials are due to ohmic resistance in the electrolyte and the anodic overpotential associated with CO_2 gas evolution. By contrast, the cathodic overpotential remains low, attributed to the high exchange current densities associated with Nd metal deposition [23].

Inert anode characteristic

Cermet materials have been identified as promising candidates for inert anodes. Inert anode investigation and research are mostly focusing on nickel ferrite spinels ($NiFeO_4$) addition of Ni, which is a good corrosion-resistant cermet material. Among various sintering methods, this study focuses on conventional sintering and spark plasma sintering (SPS) techniques.

1. Conventionally sintered anode

A conventionally sintered anode, also known as powder-sintered, is fabricated using solid-state sintering, which relies on diffusion-driven particle bonding at high temperatures. This method is widely used for ceramic and metal-oxide-based anodes due to its ability to produce dense, thermally stable structures with controlled porosity and grain growth.

The powders were thoroughly mixed with a small amount of organic binder, then uniaxially pressed and sintered in an inert atmosphere.

2. SPS anode

Spark plasma sintering, also known as Field-Assisted Sintering Technique (FAST) or Pulsed Electric Current Sintering (PECS), is a modern sintering method used to produce dense materials such as metals, ceramics, and composites. In this process, powdered material is placed in a graphite die and exposed to both uniaxial pressure and a pulsed direct current under vacuum or an inert atmosphere. The electric current causes rapid internal heating, allowing the sample to reach high temperatures in a very short time—often within minutes. This combination of fast heating and applied pressure promotes efficient densification of the material while limiting grain growth, which is important for maintaining fine microstructures [24] [25].

During sintering, Fe_2O_3 and NiO undergo solid-state reactions forming a range of mixed oxides and alloys such as Ni_xFe (a nickel-iron alloy), $Ni_xFe_{3-x}O_4$ (a non-stoichiometric spinel), and $Ni_xFe_{1-x}O$ (solid solutions), as shown in *Reaction (12)*.

$$\mathrm{Fe_2O_3 + NiO = Ni_xFe_{3-x}O + Ni_xFe_{1-x}O} \qquad (12)$$

$$\mathrm{Fe + Fe_3O_4 + NiO = Ni_xFe_{1-x} + Ni_xFe_{3-x}O_4 + Ni_xFe_{1-x}O} \qquad (13)$$

$$\mathrm{Ni + NiFe_2O_4 + NiO = Ni_xFe_{1-x} + Ni_xFe_{3-x}O_4 + Ni_xFe_{1-x}O} \qquad (14)$$

Electrolyte characteristic

In molten salt electrolysis, alkali and alkaline earth metal salts are commonly used as electrolytes because of their excellent stability and conductivity. One of their most

important features is their wide electrochemical window, which refers to the range of voltage where the electrolyte itself remains stable and doesn't undergo unwanted reactions. This means the salt components don't get reduced at the cathode or oxidized at the anode under normal operating conditions. This stability is largely due to their very negative Gibbs free energies of formation, making them hard to reduce and highly resistant to oxidation. In addition to this, these salts offer good thermal stability at high temperatures and high ionic conductivity, thanks to their strong dissociation in the molten state. Altogether, these properties make alkali and alkaline earth metal salts ideal for high-temperature electrochemical processes like neodymium electrowinning [26].

However, these electrolytes also present certain limitations. Their high melting points demand substantial energy input to achieve and maintain the molten state. Additionally, the solubility of metal ions in these salts is often limited, restricting the efficiency of electrochemical processes. Molten fluorides are also highly corrosive, posing challenges to the durability and selection of construction materials used in electrolysis cells.

The NdF_3–LiF binary phase diagram exhibits a eutectic behavior at 1 atm, with a eutectic temperature of approximately 800 °C. While pure NdF_3 melts above 1400 °C, the addition of LiF (melting point: 845 °C) significantly lowers the melting point. The eutectic composition is around 52:48 mol% NdF_3:LiF, corresponding to the lowest melting temperature in the system, as shown in Figure 3.

However, this eutectic composition does not provide sufficient Nd_2O_3 solubility for efficient electrolysis. To enhance the dissolution of Nd_2O_3 and maintain a higher concentration of electroactive neodymium species, NdF_3 is typically added in excess, often up to 85 wt%, shifting the composition away from the eutectic but optimizing for oxide solubility and electrochemical efficiency [27]. At this composition (85:15 wt% NdF_3:LiF), the minimum temperature required to keep the electrolyte fully molten is approximately 1100 °C, based on Figure 3. This operating temperature is also slightly above the melting point of Nd metal (1024 °C), enabling the electrodeposited Nd to remain in liquid form and be efficiently collected during electrowinning

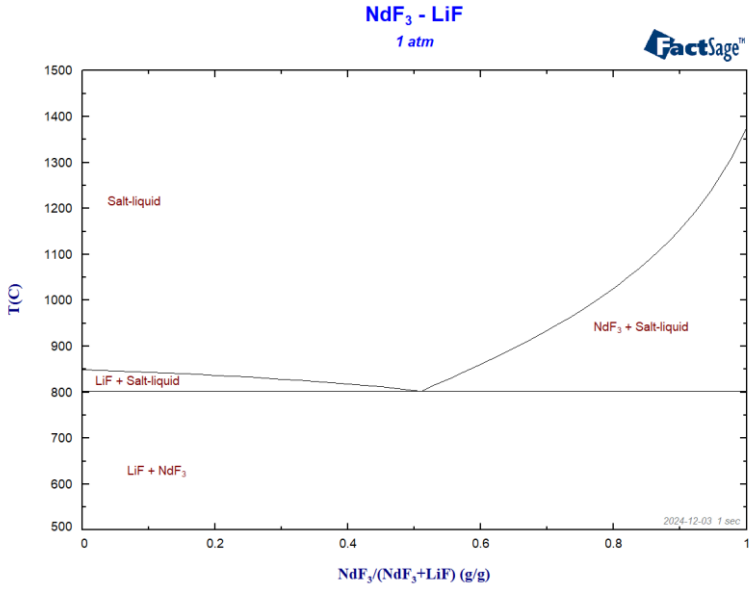

Figure 3: Binary Phase Diagram of the NdF_3–LiF System. Generated by FactSage 8.3.

The NdF_3–LiF system is preferred in Nd electrolysis due to the following advantages [26]:

- Thermodynamic stability: Fluoride-based melts, especially those containing NdF_3 and LiF, provide a wide electrochemical window because of their strongly negative Gibbs free energy of formation, ensuring the electrolyte remains stable during electrolysis [22].
- Reduced operating temperature: Adding LiF significantly lowers the melting point of the mixture, enabling operation at temperatures around 850–900 °C, which is more energy-efficient compared to using pure NdF_3.
- Improved ionic conductivity: LiF also reduces the melt's viscosity, which facilitates better ion transport and enhances the overall conductivity of the electrolyte.
- High Nd_2O_3 solubility: Compared to other fluoride systems like cryolite (Na_3AlF_6), the NdF_3–LiF mixture offers significantly higher solubility for Nd_2O_3, making it more suitable for efficient oxide feeding and consistent metal deposition.

Nd_2O_3 Solubility

The solubility behavior of Nd_2O_3 in various fluoride-based molten salt systems has been extensively studied due to its significance in rare earth electrochemical processes. Guo et al [28] summarize the previous studies on the solubility of Nd_2O_3 in LiF–MgF_2/CaF_2 and LiF–MgF_2–CaF_2/BaF_2 melts, as well as that of a series of rare earth oxides (REOs) in 81LiF–15MgF_2–4BaF_2 at 1000 °C. Their findings revealed that the chemical interaction between Nd_2O_3 and LiF was relatively weak. Rather than forming strong bonds with the

oxide, LiF primarily acted as an additive to lower the melting point and enhance ionic conductivity.

Complementary to this, Wu et al. [28] measured Nd_2O_3 solubility over a temperature range of 800–900 °C in a LiF–NdF_3–BaF_2 ternary melt. Based on their experimental data, they developed a regression equation to quantitatively describe the dependence of Nd_2O_3 solubility on both temperature and the compositions of LiF and BaF_2. Their model provided a predictive tool for solubility trends in these types of systems.

Hu [29] offered a more mechanistic perspective, exploring how both temperature and the composition of NdF_3 in LiF–NdF_3 binary melts affect the solubility of Nd_2O_3. He proposed that the dissolution of Nd_2O_3 in the melt involves the disruption of the solid's long-range order through interactions between oxide ions (O^{2-}) and neodymium fluoride complexes, particularly $[NdF_6]^{3-}$ and $[NdF_4]^{-}$. These interactions facilitate the formation of oxyfluoride species, with complexes like $[NdOF_4]^{3-}$ and $[NdOF_5]^{4-}$, as well as $[Nd_2OF_{10}]^{6-}$ and $[Nd_2OF_8]^{4-}$, being the most probable candidates.

$$Nd_2O_3 + NdF_3 + 3(x-1)LiF = 3NdOF_x^{(x-1)-} + 3(x-1)Li^+ \qquad (15)$$

The reaction illustrates that LiF primarily functions as a fluoride ion donor, while Nd^{3+} ions from NdF_3 actively support the dissolution process. Hu et al. [30] emphasized that increasing NdF_3 content in the melt enhances the formation of Nd–F complexes, which in turn promotes Nd_2O_3 solubility—a conclusion that aligns with the findings of Stefanidaki et al [31] [32] and supports the broader understanding of rare earth oxide dissolution in fluoride melts. Adding more rare earth fluoride helps rare earth oxides dissolve better, and this likely works the same way for most rare earth elements. [28] [32].

Dissolution mechanism

Different mechanism pathways have been proposed for the dissolution and electrochemical conversion of neodymium oxide in fluoride-based melts. One mechanism based on Raman spectroscopy studies was suggested by Stefanidaki et al. [32], who identified the presence of Nd^{3+} in fluoride mixtures primarily as $[NdF_6]^{3-}$ complexes. In the LiF–CaF_2–NdF_3 molten salt system, the electrodeposition of neodymium occurs via the reduction of these $[NdF_6]^{3-}$ species at the cathode, resulting in metallic neodymium deposition. This mechanism is supported by bulk electrolysis

experiments using a nickel cathode, where intermetallic phases such as NdNi, Nd_2Ni_7, and Nd_2Ni_{17} were observed, confirming neodymium's electrochemical reduction [31]. Upon addition of Nd_2O_3 to the melt, it reacts with excess fluoride and $[NdF_6]^{3-}$ to form oxyfluoride species like $[NdOF_5]^{4-}$. Even though the system's general behavior stays the same, another neodymium complex, $[NdOF_5]^{4-}$, might get involved in the reduction process under certain conditions. However, $[NdF_6]^{3-}$ is still the main ion responsible for the electrochemical reaction [33].

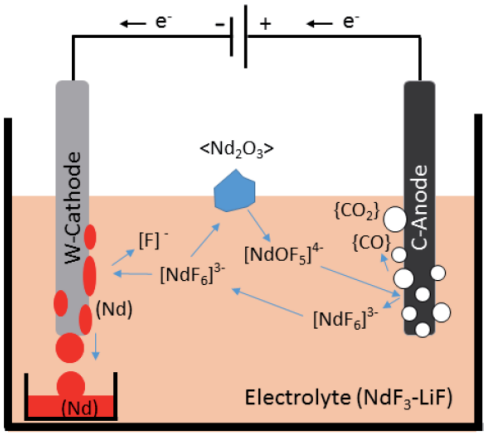

Figure 4: Dissolution and reaction mechanisms of the neodymium oxide electrolysis (Source of the illustration [4])

This understanding of the mechanism aligns with the pathway summarized in the review by Vogel [4], illustrated in Figure 4 where Nd_2O_3 reacts directly with $[NdF_6]^{3-}$ and free fluoride ions to form $[NdOF_5]^{4-}$, as shown in *Reaction (16)*. In a typical LiF–NdF_3 melt (85:15 wt%), the $[NdOF_5]^{4-}$ complex undergoes anodic oxidation, releasing oxygen gas and generating Nd^{3+} ions that are subsequently reduced at the cathode to form Nd^0, shown in *Reaction (17)* and *(18)(19)* respectively.

Dissolution: $Nd_2O_3 + [NdF_6]^{3-} + 9F^- \rightarrow 3[NdOF_5]^{4-}$ *(16)*

Anodic reaction: $3[NdOF_5]^{4-} \rightarrow 1.5\,O_2 + 3Nd^{3+} + 15F^- + 6e^-$ *(17)*

Ion dissociation: $[NdF_6]^{3-} \rightarrow Nd^{3+} + 6F^-$ *(18)*

Cathodic reaction: $2Nd^{3+} + 6e^- \rightarrow 2Nd^0$ *(19)*

These reaction pathways highlight the critical role of complex ion formation in increasing the solubility and electrochemical mobility of Nd species in the melt, thereby enhancing the efficiency of the electrowinning process. While other pathways involving intermediates such as NdOF and NdO^+ have been proposed [34] [35] [36], the mechanism summarized by Vogel [4] remains a useful reference due to its clear presentation and practical relevance to industrial electrolytes.

Understanding these reaction pathways is essential for optimizing electrolyte composition, minimizing corrosion, and improving the overall efficiency and sustainability of Nd electrowinning.

3. Material and method

3.1 Material

The experiments were conducted using different compositions of fluoride–oxide molten salt electrolyte system consisting of NdF_3 (>99,5%, Ganzhou Wanfeng Adv. Materials Tech. Co., Ltd.), LiF (97%, Thermo Scientific), and Nd_2O_3 (>99,9%, Ganzhou Wanfeng Adv. Materials Tech. Co., Ltd.) which served as a source of neodymium for experiments.

The inert anodes under investigation included nickel ferrite-based anodes ($NiFe_2O_4$), where its composition was varied in the experiment. Anodes were prepared via a two-step sintering method using NiO (99%, Thermo Scientific), Fe_2O_3 (98%, Thermo Scientific), and Ni (99.8%, Thermo Scientific). NiO and Fe_2O_3 were first sintered conventionally at 1200^{o}C in air using 4% polyvinyl alcohol (PVA) solution as an organic binder to obtain $NiFe_2O_4$ and NiO containing ceramic phase. Afterwards, metallic Ni was added to the ceramic powder containing $NiFe_2O_4$-Ni to produce final cermet anodes.

During the second sintering step, anodes were fabricated using both spark plasma sintering (SPS) and conventional sintering methods. The SPS-anode was sintered with a constant composition of 80(85$NiFe_2O_4$-15NiO)-20Ni at 950^{o}C for 10 min sintered in vacuum under 80 MPa in a cylindrical die with a diameter of 20 mm and a height of 10 mm. SPS-sintered anodes were cut in half for immersion tests, which had a semi-cylindrical shape, weighing approximately 10 g.

Conventional sintered anodes were prepared with varying nickel contents (10, 20, 30, 40, and 50 wt%) and produced at 1200 °C for 2 h in an Ar atmosphere. Initially, elongated samples were fabricated and subsequently cut into smaller pieces with a height of 10 mm to obtain uniform anode specimens. The resulting anodes had a rectangular

parallelepiped shape with a square base of approximately 5 mm on each side and a height of 10 mm, weighing approximately 2 g. The dimensions of both types of anodes are shown in Figure 5.

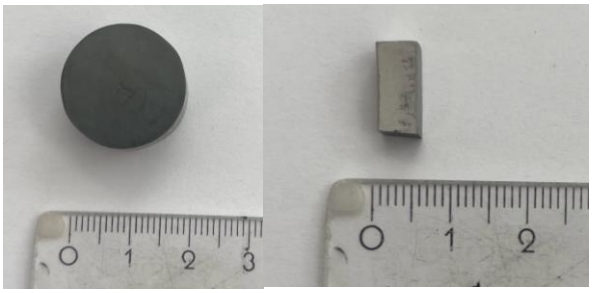

Figure 5: Dimensions of inert anodes a) SPS-sintered anode, b) conventionally sintered anode

To evaluate anode corrosion, an immersion test is conducted. Since no external current is applied, the test focuses entirely on the material's natural corrosion behavior, without interference from electrochemical reactions caused by an applied voltage.

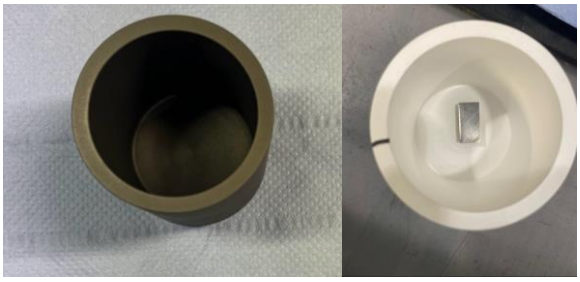

Figure 6: a) Graphite crucible b) Boron Nitride crucible

The electrolyte pre-melting and immersion tests were conducted using a graphite and BN (SITUS Technicals) crucibles with an outer diameter of 60 mm, an inner diameter of 50 mm, an outer height of 70 mm, and an inner height of 65 mm, shown in Figure 6.

3.2 Method

3.2.1 Immersion test

The immersion test is one of the practical tests to determine corrosion of the material of interest and the liquid or molten medium under specific operating conditions. Without any applied current, the test purely evaluates the corrosion of the material rather than electrochemical degradation caused by an external potential [37].

Since no current is applied, the maximum possible corrosion of the anode is observed in the immersion test due to the absence of a protective oxide layer in the electrolysis process. At the anode, oxidation occurs, the oxygen gas is released, and it reacts with the anode, forming a passivation layer during molten salt electrolysis. This passivation

layer slows down further corrosion by creating a barrier between the molten salt and the anode material [38].

For the pre-melting stage, NdF_3, LiF, and Nd_2O_3 powders were accurately weighed based on the target composition to obtain a total mass of 200 g and were subsequently homogenized by thorough mixing. In the investigation of different anode materials, the electrolyte composition was kept constant at 2 wt% Nd_2O_3, 83.3 wt% NdF_3, and 14.7 wt% LiF. To study the effect of electrolyte composition, the NdF_3–LiF weight ratio was systematically varied as 45:55, 55:45, 65:35, 75:25, and 85:15 (wt%), with no addition of Nd_2O_3. Furthermore, to evaluate the influence of Nd_2O_3 concentration on corrosion behavior, its content was varied at 0, 0.5, 1.0, 1.5, and 2.0 wt% while maintaining a fixed NdF_3:LiF ratio of 85:15 (wt%). The mixture in the graphite crucible was dried at 110°C for 24 hours to remove any residual moisture and pre-melted in a chamber furnace (HTK 25GR/25-2G, Carbolite Gero) at 1100°C for 2 h under an Ar atmosphere to reduce the powder volume.

200 g of molten salt mixture was used to submerge the inert anode specimen in a graphite crucible for the immersion test. This setup was placed in a chamber furnace and held under an Ar atmosphere. The anodes were tested in the molten salt at temperatures up to 1100 °C for a duration of 6 h.

3.2.2 Neodymium electrolysis

The salt mixture of 14.7 wt.-% LiF (97%, Thermo Scientific), 83.3 wt.-% NdF_3 (>99,5%, Ganzhou Wanfeng Adv. Materials Tech. Co., Ltd.), and 2 wt.-% Nd_2O_3 (>99,9%, Ganzhou Wanfeng Adv. Materials Tech. Co., Ltd.) was dried at 110 °C for 24 h and then melted in a chamber furnace (HTK 25GR/25-2G, Carbolite Gero) at 1100 °C for 2 h under an Ar atmosphere for the volume reduction of the powder.

The 1.2 kg of crushed pre-melted electrolyte was first placed into a smaller carbon crucible (outer diameter of 70 mm and an inner diameter of 50 mm). Additionally, a molybdenum crucible was positioned beneath the cathode rod to collect the deposited liquid metallic neodymium. To prevent potential leakage of the molten electrolyte, this crucible was placed inside a larger protective graphite crucible (outer diameter of 100 mm and inner diameter of 80 mm). The graphite crucible assembly was then inserted into a steel cell, providing a sealed reactor during the high-temperature process.

For the electrowinning process, a tungsten rod cathode (diameter of 3 mm), a conventionally sintered inert anode (a sample with a 5 mm square base and 65 mm height) containing 30% Ni, and a tungsten wire reference electrode (diameter of 1 mm)

were employed. All electrodes were enclosed in alumina tubes for insulation. In addition to the primary temperature monitoring, three thermocouples were attached to the lid of the setup to measure the off-gas temperature, the temperature around the lid, and the adjustable temperature within the electrolyte, using a type K thermocouple housed in a 6 mm steel sheath. Before electrolysis, all components were thoroughly dried. The positioning of the electrodes and thermocouple is shown in Figure 7.

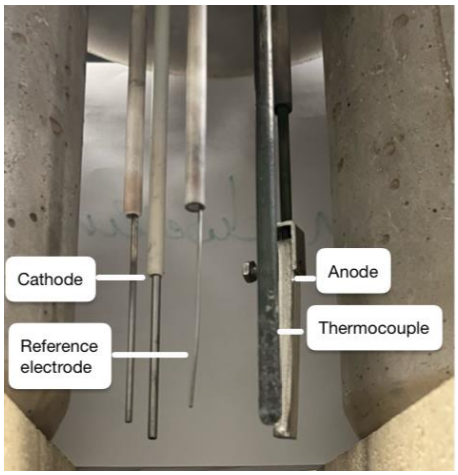

Figure 7: Electrode setup mounted on the lid of the electrochemical cell, showing the cathode, reference electrode, anode, and thermocouple before electrowinning.

Before electrolysis, the cell was evacuated to create a vacuum and remove air. It was then purged with Ar four times to ensure complete air removal. The electrolysis was performed at 1070 °C for 2 hours in a resistance furnace. The furnace was preheated to 1070 °C before electrode insertion. To ensure safe operation, the lid, upper cell components, and related fittings were continuously cooled. An Ar gas flow of 120 L/h was maintained throughout the experiment.

The electrodes were immersed in the molten electrolyte. After 2 h, the electrodes were lifted to prevent them from solidifying inside the electrolyte. In Figure 8, the Nd electrowinning cell set is shown.

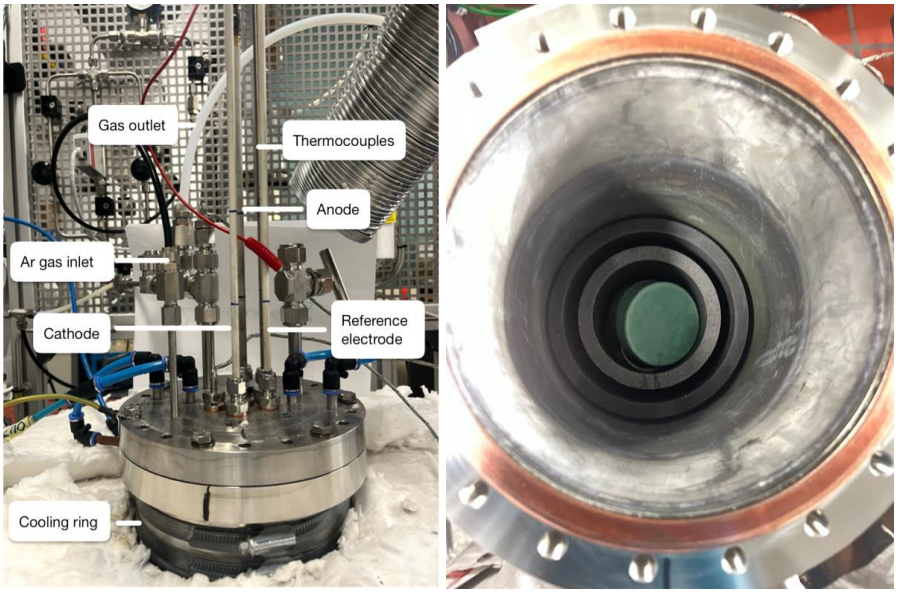

Figure 8: Neodymium electrowinning: a) Cell setup with lid and components, b) Inside the cell – carbon crucible containing pre-melted electrolyte

The composition of the off-gas was continuously monitored using Fourier-Transform Infrared Spectroscopy (FTIR) (Matrix-MG2, Bruker), which measured CO, CO_2, CF_4, C_2F_6, HF, and H_2O. The electrowinning was powered by a DC rectifier. Off-gases were filtered and washed through a sodium hydroxide (NaOH) solution for neutralization.

3.2.3 ICP-OES measurement

Inductively Coupled Plasma Optical Emission Spectroscopy (ICP-OES) is an analytical technique used to determine the composition of specific elements in a sample. The method utilizes extremely hot plasma (Ar plasma) to excite atoms and ions. As electrons transition from their excited state back to lower energy levels, they emit photons at characteristic wavelengths. These wavelengths are detected and, after calibration with known element concentrations, the emission intensity is measured to quantify the elements present. This technique enables the highly accurate detection of trace elements. ICP-OES samples are introduced in an aqueous solution with appropriate dilution to ensure precise measurements [39, 40].

After the immersion test, the electrolyte was analyzed using ICP-OES (Agilent 725-ES, Varian) to determine the concentrations of Nd, Ni, Fe and Li. A solidified electrolyte was milled in a disc mill for 2 min and dissolved in HCl for microwave leaching before analysis. 8 M HCl was used as a lixiviant, which was prepared from concentrated HCl (37 wt%, VWR Chemicals). A 0.2 g powder sample was dissolved in 15 mL of lixiviant.

The results indicate the extent of anode dissolution in the electrolyte, providing insight into its inertness.

3.2.4 SEM/EDX measurement

Scanning Electron Microscopy with Energy Dispersive X-ray Spectroscopy (SEM/EDX) is a surface analytical technique that scans a sample's surface using a focused electron beam. This interaction generates signals due to electron-atom interactions, producing high-resolution images of the sample at the microscopic level.

During the measurement, atoms are excited by an electron beam and emit their characteristic X-rays for each element. The EDX system detects these X-rays, identifies their energy, and quantifies elements present in the sample. This method is particularly useful for determining corrosion depth and analyzing anode dissolution [41, 42].

After the immersion tests, the anode was carefully separated from the solidified electrolyte using a chisel and a rubber hammer. The sample was then cut cross-sectionally and embedded in PolyFast—a phenolic resin with graphite filler—using a hot mounting press at 170 °C and 200 N pressure. PolyFast was selected due to its low shrinkage and high electrical conductivity, making it suitable for SEM analysis. After embedding, the samples were ground with SiC paper under water cooling and polished using DiaDuo diamond suspensions (9 µm, 3 µm, 1 µm) stepwise, which contain monocrystalline diamonds in a water-based solution. Prior to SEM examination, the polished sample surface was sputter-coated with a thin layer of Au to improve conductivity and image resolution.

SEM-EDX analysis was conducted using an Ultra55 (Zeiss) microscope to evaluate surface morphology and elemental distribution. Corrosion zone depth was manually approximated using the SEM software's cursor tool. Total corrosion depth was determined from EDX line scan data, calculated as the distance between the point where Nd content significantly decreased and the point where Ni was first detected.

Three EDX line scans were performed along the upper middle region of the sample, and the average of these measurements was used to improve accuracy. In addition, EDX spot analyses were carried out to determine the elemental composition at selected phases. Elemental ratios obtained from these spot analyses were used to identify the phases present. Understanding these phases provides valuable insight into the corrosion mechanisms of the inert anodes.

3.2.5 XRD measurement

X-ray Diffraction (XRD) is an analytical technique used to identify the crystalline structure, phase composition, and lattice parameters of materials. The working principle is that the X-ray source produces X-ray radiation, which is directed at the sample, and

X-rays interact with the crystal lattice. If the sample is crystalline, the atomic planes act like mirrors, reflecting the X-rays at specific angles according to **Bragg's Law**:

$$n\lambda = 2dsin\theta$$

n = integer (order of reflection)

λ = X-ray wavelength

d = interplanar spacing of the crystal lattice

θ = diffraction angle [43]

Diffracted X-ray intensity is recorded in the detector as a function of diffraction angle, θ. The resulting XRD pattern (diffractogram) consists of characteristic peaks corresponding to specific interplanar spacings in the crystal structure [44]. Each material has a unique set of peaks, allowing phase identification by comparing the pattern to reference databases such as the International Centre for Diffraction Data (ICDD).

A representative portion of the powder electrolyte was then placed into XRD sample holders. To ensure a flat and level surface, the sample was gently pressed using a glass plate with a flat surface, and excess material around the holder was cleaned. The prepared sample was then analyzed using XRD to identify the phase composition in the electrolyte. The results from XRD were analyzed using the Interfaith Center for Sustainable Development (ICSD) database as a reference, and the peaks were visualized in Origin software.

4. Result and discussion

This section presents the experimental findings on the corrosion behavior of nickel ferrite-based inert anodes in NdF_3-LiF molten salt. The results were structured into two main parts: (i) the immersion test results, which evaluate the chemical stability of various anode compositions, various electrolyte compositions as well as anode sintering conditions, under no applied current, and (ii) the electrolysis performance of the promising nickel ferrite-based anode. Key parameters such as corrosion depth, anode dissolution, and post-exposure phase composition were analyzed to assess the suitability of the tested anodes for application in the neodymium electrowinning.

4.1 Immersion test result

4.1.1 Crucible: Boron nitride crucible vs Graphite crucible

Carbon is considered a strong reducing agent, particularly in high-temperature processes where it reduces various metal oxides such as NiO, Fe_2O_3, and CuO to their respective metals [45]. Therefore, graphite crucibles may not be ideal for the immersion tests aimed at evaluating the corrosion behavior of $NiFe_2O_4$-based anodes. Dissolved metal species may be reduced on the inner wall of the graphite crucible, altering the actual corrosion results. For this reason, BN crucible was considered a potentially better alternative due to its chemical inertness.

To evaluate this, both BN and C crucibles were tested under identical conditions. The electrolyte used contained 2 wt% Nd_2O_3, 83.3 wt% NdF_3, and 14.7 wt% LiF, and the anodes were produced via SPS.

Table 3: ICP-OES results for electrolytes after 6 h immersion at 1100°C in graphite and BN crucibles. Electrolyte composition: 2 wt% Nd_2O_3, 83.3 wt% NdF_3, and 14.7 wt% LiF

Crucible	Measured Li %	Measured Nd %	Measured Ni %	Measured Fe %
C	4.21	51.01	0.025	0.055
BN	3.605	49.925	0.185	0.275

As shown in *Table 3*, there is a significant difference in the measured Ni and Fe concentrations between the two crucibles. Given that both the electrolyte composition and anode material were identical, the dissolved metal content should have been comparable under constant conditions. However, when the graphite crucible was used, the Ni and Fe concentrations were significantly lower. This is likely due to the reducing nature of carbon, which promotes the reduction of dissolved metal ions on the crucible wall, as shown in Figure 9a. In contrast, the BN crucible maintained higher metal concentrations in the electrolyte, suggesting that reduction did not occur.

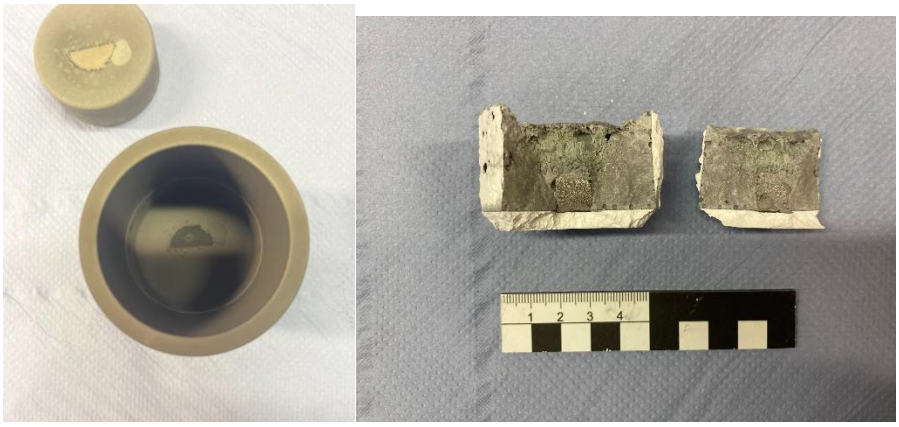

Figure 9: Crucibles after a 6-hour immersion test at 1100 °C in an electrolyte composed of 2 wt% Nd_2O_3, 83.3 wt% NdF_3, and 14.7 wt% LiF. a) *Circular patch observed on the inner wall of the carbon b) Fractured boron nitride (BN) crucible*

However, one drawback of using BN crucibles was noted after the test: the solidified electrolyte adhered strongly to the crucible walls and could not be removed easily. Despite attempts to dislodge it using a rubber hammer, the BN crucible broke due to its brittleness, indicating that BN crucibles are single-use, shown in Figure 9b. The reason for the adhesion is unclear, but it could be related to a possible reaction between the crucible material and the molten NdF_3–LiF electrolyte [46]. Some BN crucibles may contain boron oxide impurities, which could potentially react with the melt and contribute to the strong adhesion.

4.1.2 Anode: SPS condition

In this study, the behavior of SPS-sintered $NiFe_2O_4$–NiO–Ni anodes was evaluated in an electrolyte composed of Nd_2O_3 (2 wt%), NdF_3 (83.3 wt%), and LiF (14.7 wt%) using immersion tests. The sintering parameters, including temperature (950 °C, 1000 °C, and 1050 °C) and time (5, 10, and 20 minutes), were varied to investigate their influence on anode performance.

Table 4: SPS anode sintering condition and electrolyte composition

Number of experiments	Anode				Electrolyte	
	SPS Condition		Ni	$NiO\text{-}NiFe_2O_4$	Nd_2O_3	$NdF_3\text{-}LiF$
	Temperature	Time				
1	950°C	5 min	20%	15%-85%	2%	85%-15%
2	1000°C	5 min				
3	1000°C	10 min				
4	1000°C	20 min				
5	1050°C	10 min				

SEM/EDX result

Corrosion behavior of the SPS-sintered $NiFe_2O_4$-NiO-Ni inert anodes was examined after immersion in molten NdF_3–LiF electrolyte. The corrosion depth was analyzed using cross-sectional SEM imaging and EDX line scanning. It was measured at three distinct positions from the top surface, with the region directly exposed to the electrolyte without interacting with the carbon crucible providing an average depth considered as the corrosion depth.

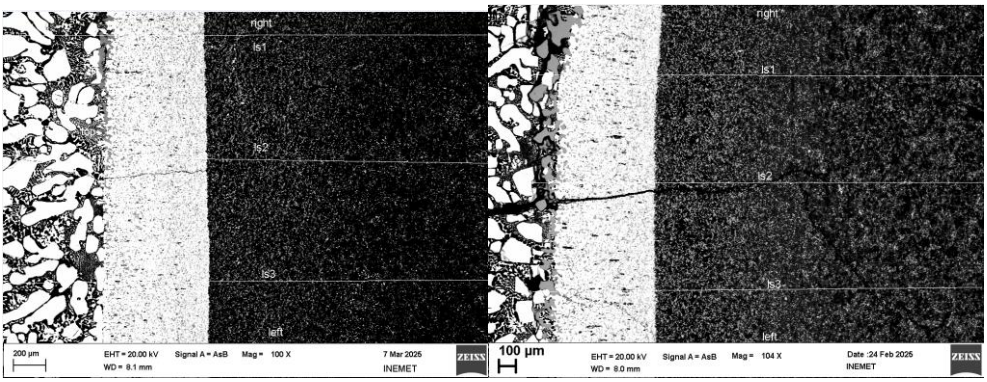

Figure 10: Line scanning on post-anode surfaces at 100x magnification, sintered at a) 1050 °C for 10 min and b) 1000 °C for 5 min

Each corroded sample exhibited a layered structure comprising three distinct corrosion zones, as shown in Figure 10. These layers were distinguished based on microstructural contrasts in SEM and variations in elemental composition detected via EDX. While all samples revealed similar corrosion phases, their distribution and thickness varied with sintering conditions.

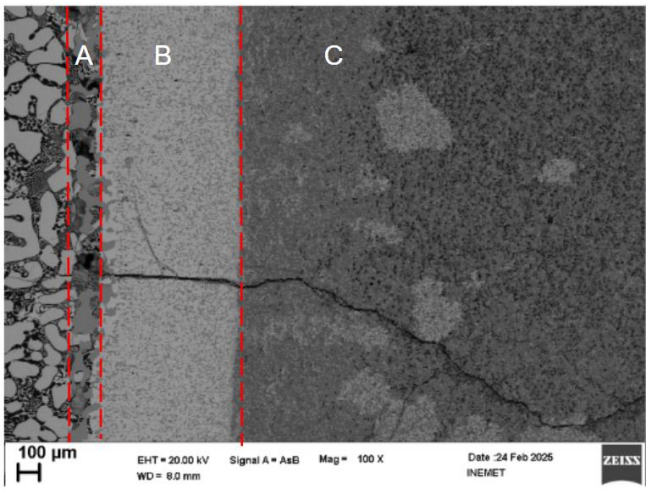

Figure 11: Backscattered (BSE) image of different zones of the anode sintered at 1000 °C/10 min after a 6 h immersion test at a magnification of 100x.

- **Zone A**: The outermost layer mainly consisted of metallic phases like the Ni-Fe alloy, in which NdF_3-LiF salts solidified in the pores. This zone reflects direct interaction with the electrolyte and shows significant dissolution.
- **Zone B**: This zone contained a mixture of metallic Ni_3Fe and $NdO_{0.67}F_{1.66}$, and $FeNdO_3$, representing a transitional interface where partial conversion of oxides occurred.
- **Zone C**: This region corresponds to the unreacted bulk of the inert anode, containing a mixture of Ni-Fe alloy and $NiFe_2O_4$ phases, preserving the integrity of the original structure.

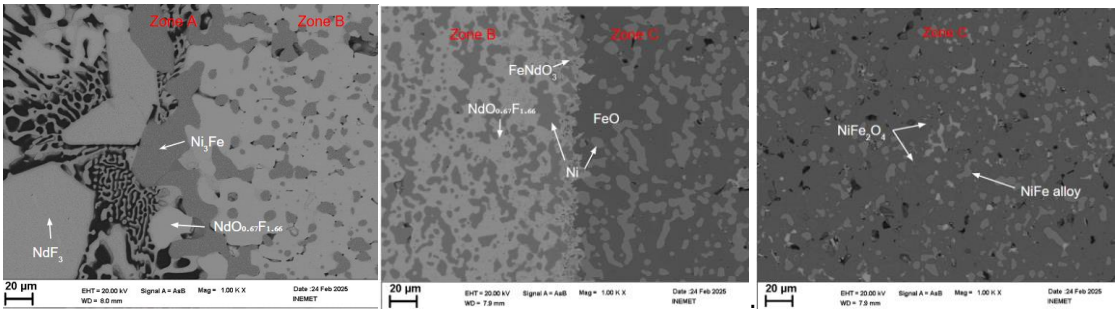

Figure 12: Spot analysis of the post-anode sintered at 1050°C for 10 min at 1000x magnification, indicating a) Electrolyte and Zone A regions, b) Zone B and Zone C regions, c) Zone C region

In Figure 12a, the light-grey regions primarily consist of Nd containing phases such as NdF_3 and $NdO_{0.67}F_{1.66}$, while the darker grey areas correspond to the Ni_3Fe phases from the anode material. At the interface between Zones B and C, as shown in Figure 12b, Ni-Fe alloy phases were detected in both regions; however, the $NdO_{0.67}F_{1.66}$ phase was only observed in Zone B. This suggests that Nd penetrated the anode structure up to this

boundary, marking the extent of its diffusion, referred to as the corrosion depth. In the deeper region of Zone C shown in Figure 12c, the light-grey areas were enriched in Ni, while the dark-grey regions were identified as $NiFe_2O_4$, the original ceramic phase of the anode.

Based on the observed phase changes and elemental distribution**,** it can be concluded that the $NiFe_2O_4$ phase collapses or degrades upon interaction with the molten electrolyte. This is supported by the absence of the $NiFe_2O_4$ phase in the corroded regions, where a Ni-rich zone was detected instead. The preferential degradation of the $NiFe_2O_4$ phase suggests its limited stability in the corrosive molten salt environment, while the metallic phase remains stable in aggressive environments.

To further support the identification of corrosion zones and clarify elemental migration during the corrosion process, EDX line scan analysis was performed across the anode cross-section.

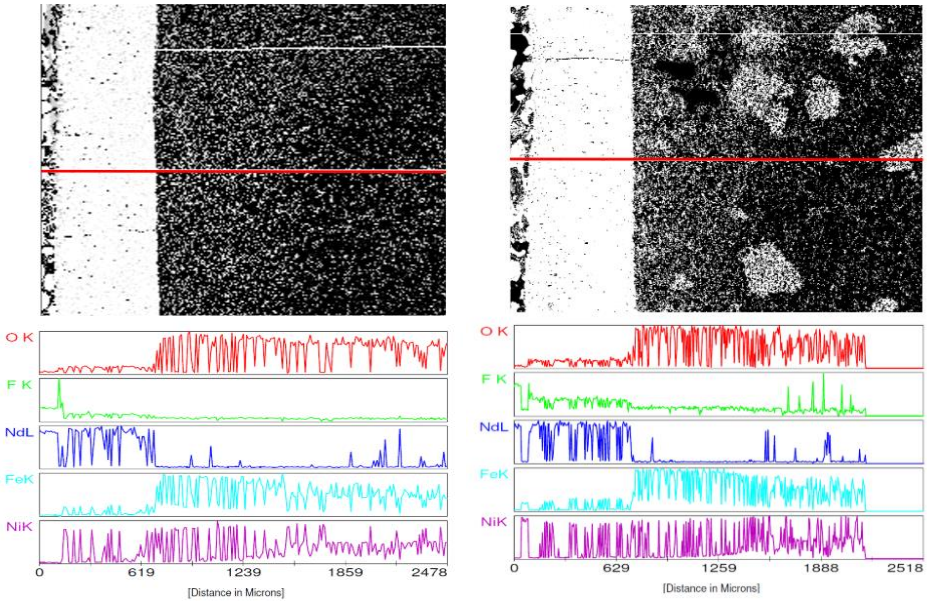

Figure 13: SEM micrographs and EDX scan analyses of inert anodes at 100x magnification. Sintering conditions of the anodes a) 1050 °C for 10 min and b) 1000 °C for 10 min

Figure 13 presents EDX line scan data across the corroded anodes, showing the elemental distribution along a cross-sectional line of the anode. Ni was detected throughout the corrosion profile, with a constant signal intensity in Zone C, while Fe and O signals notably increased in the transition from Zone B to C. Conversely, Nd concentration was high in Zones A and B but dropped sharply in Zone C, indicating limited penetration into the bulk structure.

The presence of metallic Ni_3Fe and oxyfluoride phases points toward a corrosion mechanism that preferentially depletes oxygen and metal cations, leading to the breakdown of the ceramic structure.

Corrosion depths were evaluated using both morphological and elemental measurements. The measured corrosion depth was determined by manually measuring the extent of Zones A and B on SEM images. The corrosion depth was defined as the distance between the initial detection of Ni (marking metal-rich zones) and the decline in Nd signal (indicating the corrosion front limit) in the EDX line. Measurements were taken from three line scans spaced approximately 7 µm apart, and the final corrosion depth was reported as the average of these values

Table 5: Corrosion depth of SPS-sintered anodes after a 6-hour immersion test at 1100°C. Electrolyte composition: 2 wt% Nd_2O_3, 83.3 wt% NdF_3, and 14.7 wt% LiF

Sintering condition		Measured depth (µm)		Total depth measured from SEM images (µm)	Total depth calculated from EDX scan (µm)
Temperature (°C)	Holding Time (min)	Zone A	Zone B		
950	5	211.5	608.2	839.5 ± 6.6	805
1000	5	261.5	517.1	766.91 ± 10.3	766.8
1050	10	111.6	608.2	694.14 ± 15.3	719.8
1000	10	173.3	634.6	743.83 ± 4.3	790.3
1000	20	202.7	617	819.7 ± 1.6	803.2

Table 5: Corrosion depth of SPS-sintered anodes after a 6-hour immersion test is summarized in Table 5**,** where the measured and calculated corrosion depths for all sintering conditions. The sample sintered at 1050°C for 10 min exhibited the lowest total corrosion depth, suggesting enhanced corrosion resistance due to improved densification and reduced pore connectivity. In contrast, the 950°C for 5 min sample showed the deepest corrosion, attributed to insufficient densification and increased surface area available for molten salt attack.

At 1000°C, holding time significantly influenced corrosion depth. The 5 min sintered sample showed a relatively high corrosion depth, the lowest total corrosion was 766.8 µm, likely due to insufficient grain growth and high surface reactivity. Prolonging the holding time to 10 and 20 min slightly reduced corrosion resistance, possibly due to abnormal grain growth or microcrack development, which allowed deeper melt penetration. Although density was not directly measured in this study, longer holding

times during sintering are generally known to promote densification and reduce porosity, as reported in previous studies [47]. This densification may influence the corrosion behavior of the anode material by altering electrolyte penetration and interfacial reactions.

ICP-OES result

After the immersion test, the solidified electrolyte was milled, and samples were analyzed using ICP-OES to quantify the concentrations of Li, Nd, Ni, and Fe in the electrolyte.

Table 6: ICP-OES results for electrolytes after 6 h immersion at 1100°C with anodes sintered under different SPS conditions. Electrolyte composition: 2 wt% Nd_2O_3, 83.3 wt% NdF_3, and 14.7 wt% LiF

No	Sintering condition		Initial Li %	Measured Li %	Initial Nd%	Measured Nd %	Measured Ni %	Measured Fe %
	Temperature °C	Holding time (min)						
1	950	5	3.96	4.21	61.39	51.01	0.025	0.055
2	1000	5	3.96	4.09	61.39	48.835	0.03	0.06
3	1000	10	3.96	3.725	61.39	42.965	0.01	0.07
4	1000	20	3.96	3.86	61.39	38.72	0.01	0.05
5	1050	5	3.96	3.98	61.39	43.805	0.045	0.05

For the Li content, no significant change was observed compared to the initial composition. This is expected, as Li primarily acts as a fluoride ion (F^-) donor in the molten salt and does not significantly participate in corrosion reactions.

In contrast, the Nd content showed a slight decrease after the immersion test. This trend supports the earlier SEM-EDX analysis, which revealed Nd-containing phases such as NdF_3 and NdOF infiltrating the anode. On the other hand, the leaching process was not entirely successful, likely due to incomplete dissolution of the samples in acid.

Most notably, Fe was found in higher concentrations than Ni in all electrolyte samples. The possible explanation is that Ni was reduced to its metallic form by the carbon crucible, therefore remaining as solid metal instead of dissolving into the electrolyte. This could explain the lower Ni content in the electrolyte.

XRD result

Figure 14 presents the XRD patterns of electrolytes collected after immersion tests using SPS-sintered anodes. The dominant phases identified in all samples were LiF, NdF_3,

and $NdO_{0.67}F_{1.66}$. Importantly, no crystalline phases containing Ni or Fe were detected. This absence suggests that the Ni and Fe released from the anodes during corrosion did not remain dissolved in the molten electrolyte, but were instead likely reduced and deposited onto the graphite crucible wall.

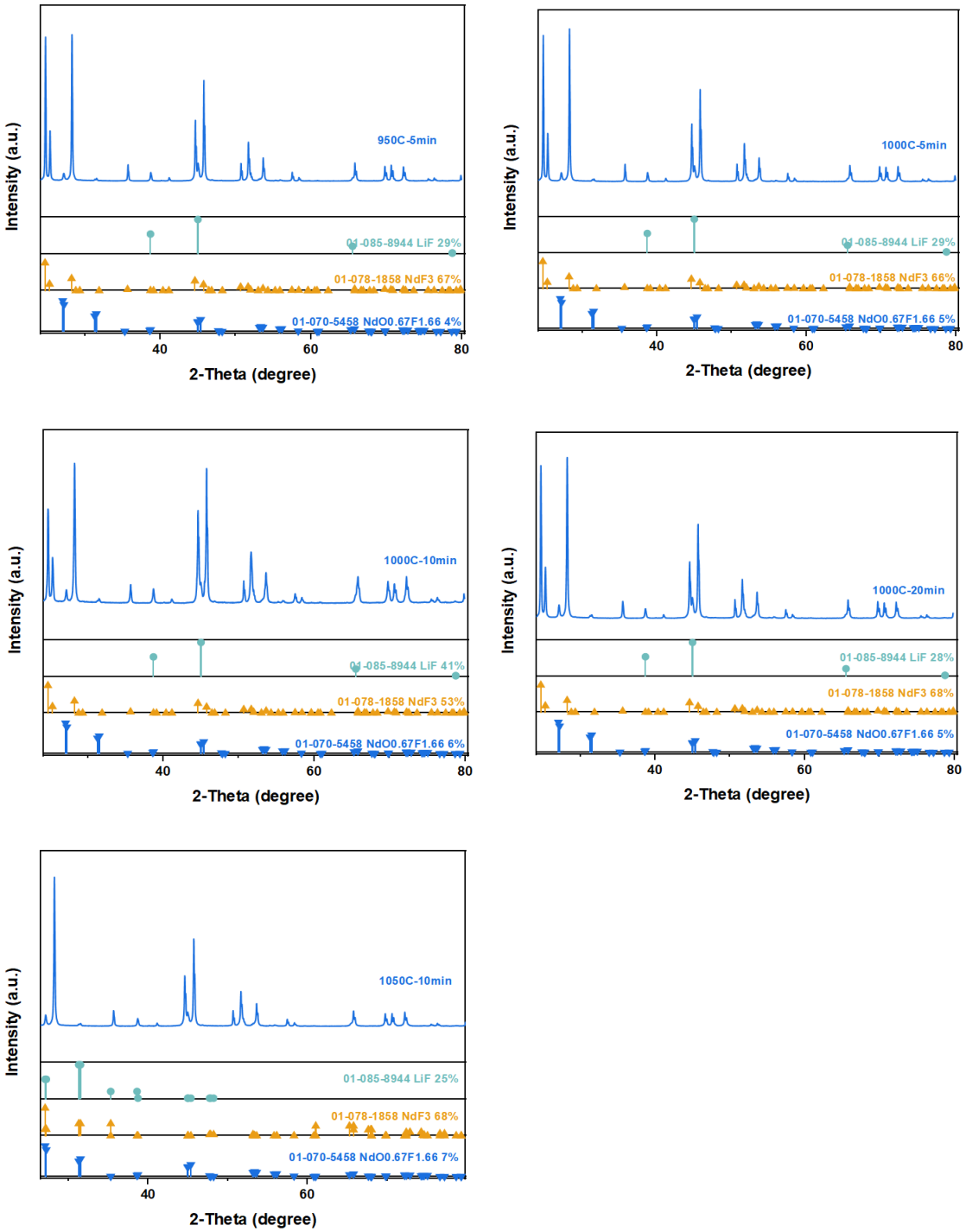

Figure 14: XRD patterns of electrolytes after 6 h immersion tests at 1100°C *with SPS-sintered anodes. Electrolyte composition: 2 wt% Nd_2O_3, 83.3 wt% NdF_3, and 14.7 wt% LiF*

4.1.3 Effect of varying Ni content in conventionally sintered anodes

To investigate the influence of Ni content on the corrosion behavior of the anodes, a series of immersion tests were conducted using conventionally sintered anodes with varying Ni concentrations: 10, 20, 30, 40, and 50 wt%. The elongated sintered anodes were cut into 2 cm long segments for testing. The electrolyte composition was kept constant at 85:15 wt% NdF_3:LiF, and addition of 2 wt% Nd_2O_3 for all experiments.

SEM/EDX result

All of the conventionally sintered anodes, regardless of Ni content, appeared quite porous. As shown in Figure 15, the core of each anode was more porous than the outer regions. This is most likely due to the shape and pressing process used before sintering. Since the anodes were pressed into elongated shapes, the sides experienced more pressure during compaction, resulting in a denser structure there. In contrast, the center received less compression, leading to increased porosity. This uneven density is common in conventionally sintered samples. It is important to note that in the initial (as-prepared) anode material, no $NiFe_2O_4$ or NiO phases were detected. Instead, only a metallic Ni–Fe alloy phase was present. This observation suggests that during the sintering process, the expected oxide phases either decomposed or were reduced, although the mechanism behind this transformation remains unclear. Interestingly, in samples with a lower Ni content, residual oxide phases were still observable in the core region. However, in samples with higher Ni content, these oxides were absent throughout the entire structure.

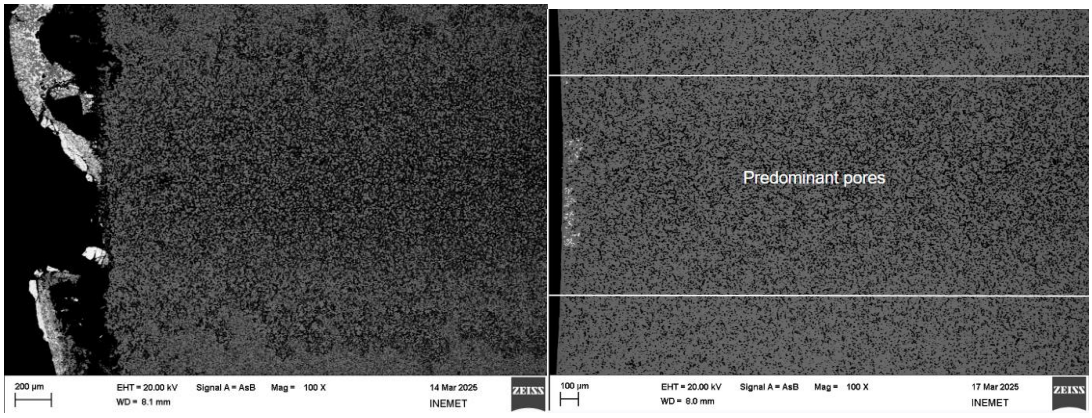

Figure 15: Conventionally sintered anodes after 6 h immersion test using anodes with a) 10% Ni content, b) 30% Ni content at 1100°C. Electrolyte composition: 2 wt% Nd_2O_3, 83.3 wt% NdF_3, and 14.7 wt% LiF

After the immersion test, only the sample with 20% Ni showed visible electrolyte penetration, shown in Figure 16. This was likely not due to chemical attack, but rather due to high porosity. The increased porosity is attributed to the fact that this sample was cut from the middle section of a longer sample, where densification may have been less uniform.

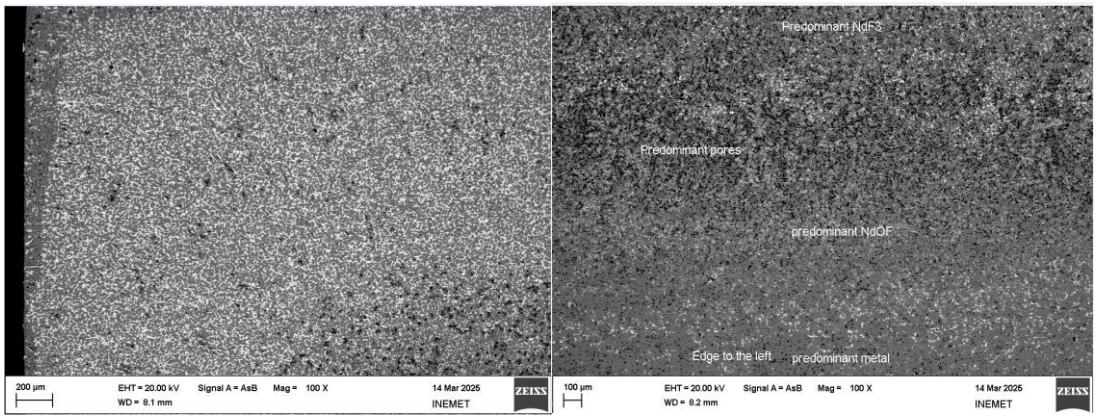

Figure 16: Electrolyte penetration observed in the conventionally sintered anode with 20% Ni content a) top-middle region, b) left side of the core.

No visible differences or distinct corrosion zones existed in any of the anodes under this condition. However, slight electrolyte penetration (around 70 µm) was observed in the 30% Ni anode shown in Figure 17**.** EDX spot analysis revealed that the light-gray and white areas correspond to NdF_3 and $NdOF_x$ phases, while the gray regions are the NiFe alloy with a Ni/Fe atomic ratio ranging from 4.5 to 6.2. The darkest regions were identified as pores. These phases were present before the immersion test, suggesting that they were part of the initial structure and not the result of corrosion.

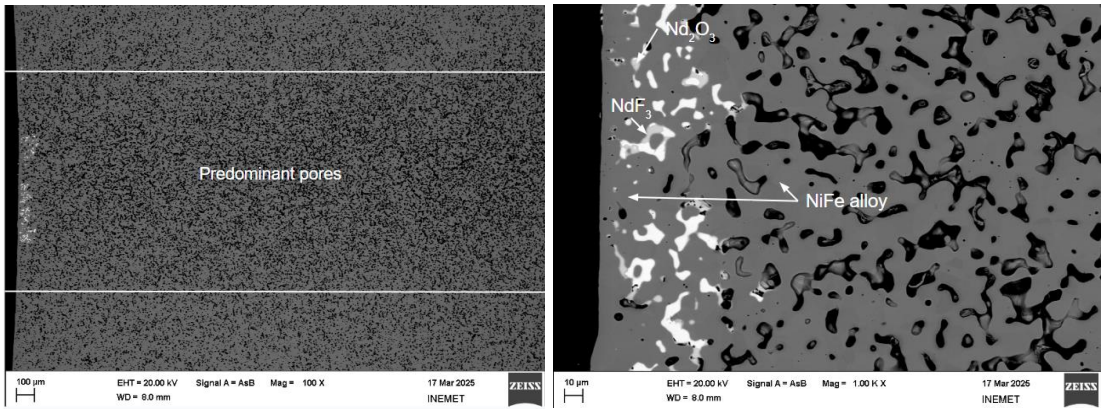

Figure 17: 30% Ni anode (a) Top surface at 100× magnification; (b) Top-middle region where the electrolyte penetrated the anode, at 1000× magnification

Varying the Ni content did not result in a clear difference in corrosion depth or the formation of significantly different corrosion-related phases. This suggests that, under

the tested conditions, the overall corrosion behavior of the conventionally sintered anodes was not strongly influenced by Ni content alone.

ICP-OES result

ICP-OES was used to measure the concentrations of Li, Nd, Ni, and Fe in the electrolyte after the immersion tests. The results are summarized in Table 7**.**

Table 7: ICP-OES result of electrolyte composition after 6 h immersion test using anodes with different Ni contents at 1100°C. Electrolyte composition: 2 wt% Nd_2O_3, 83.3 wt% NdF_3, and 14.7 wt% LiF

No	Ni content	Initial Li %	Measured Li %	Initial Nd%	Measured Nd %	Measured Ni %	Measured Fe %
1	10%	3.96	3.88	61.39	48.64	<0.01	0.01
2	20%	3.96	3.95	61.39	36.27	<0.01	0.03
3	30%	3.96	3.91	61.39	57.8	0.01	0.01
4	40%	3.96	3.94	61.39	47.21	<0.01	<0.01
5	50%	3.96	3.96	61.39	46.13	<0.01	0.01

Both Ni and Fe concentrations in the electrolyte were very low (≤ 0.01%), suggesting that the anode material remained stable and did not significantly dissolve during the immersion tests. This indicates that the corrosion of the anodes was minimal, and the dissolution of metal ions into the electrolyte was negligible under the given test conditions.

XRD result

XRD analysis of the electrolyte after the immersion tests confirmed the presence of LiF, NdF_3, and $NdO_{0.67}F_{1.66}$ phases in all samples. No additional phases were detected from the electrolyte after the 6 h immersion test.

The results indicate that varying the Ni content in the anode composition did not lead to the formation of new phases, nor did it significantly affect corrosion behavior, as evidenced by the stable Ni and Fe concentrations and consistent XRD patterns.

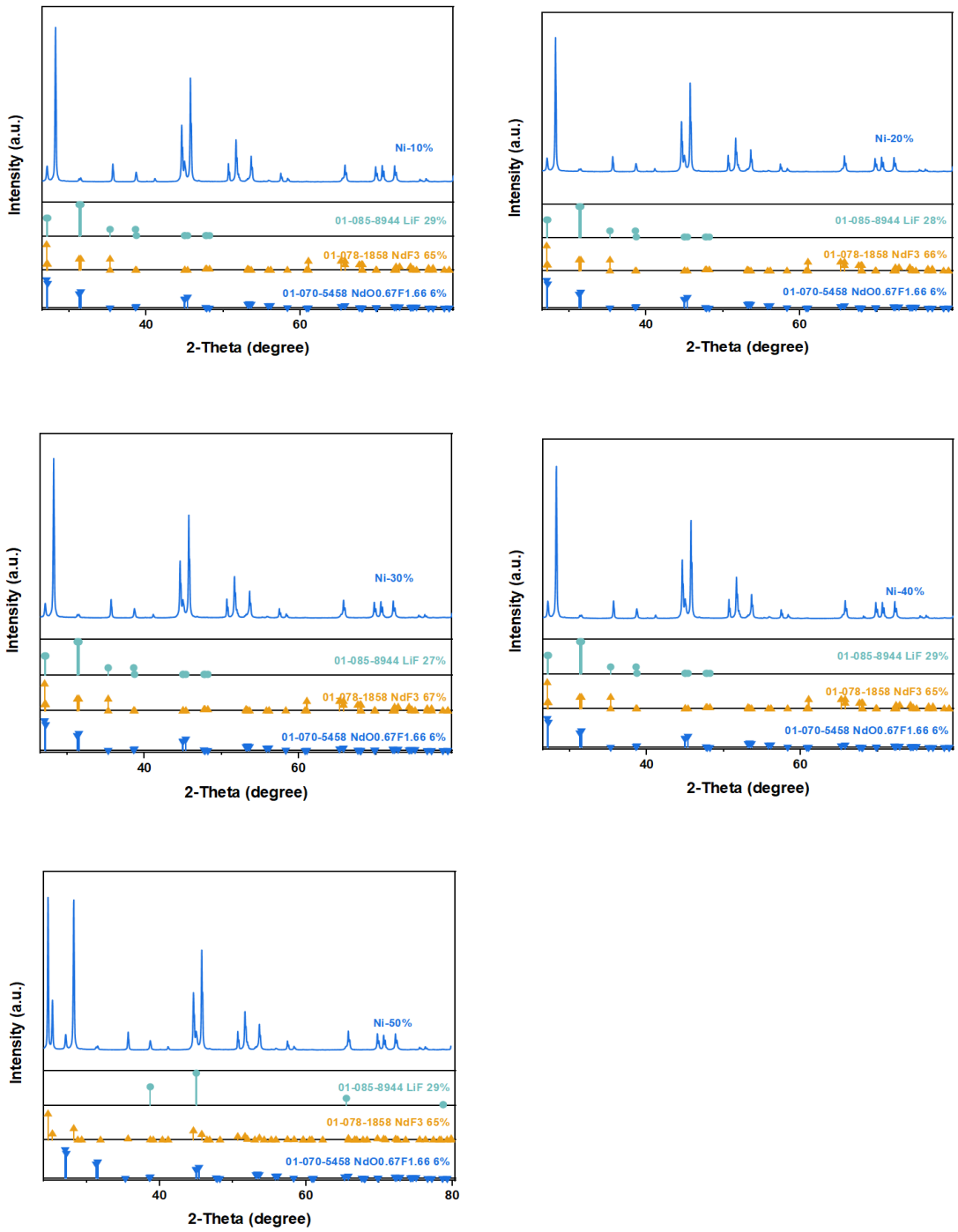

Figure 18: XRD analysis of phases in electrolytes after immersion tests with anodes of varying Ni content.

Within the tested range (10–50 wt%) variations in Ni content in conventionally sintered anodes do not have a noticeable effect on corrosion in the 85:15 wt% NdF_3:LiF electrolyte. The anodes remained chemically stable, and no additional corrosion-related phases were observed. From a theoretical standpoint, the lack of reaction is because Ni and Fe are less active than Nd and Li**.** Their lower electrochemical reactivity means they

are not easily fluorinated or oxidized in the NdF_3–LiF melt [48]. The electrolyte conditions are not enough to overcome the thermodynamic stability of Ni and Fe in this environment.

4.1.4 Effect of NdF_3–LiF Composition

This section investigates the influence of electrolyte composition on the corrosion behavior of the anode by varying the NdF_3–LiF ratio, without adding Nd_2O_3. All experiments were conducted using a conventionally sintered anode with the composition 80(85$NiFe_2O_4$–15NiO)–20Ni (wt%). Five different electrolyte compositions were tested: NdF_3:LiF mass ratios of 45:55, 55:45, 65:35, 75:25, and 85:15. These variations were selected to examine how increasing NdF_3 content affects the chemical stability and corrosion resistance of the anode under no applied current. The results provide insight into the relative aggressiveness of each melt composition.

SEM/EDX result

In all tested NdF_3–LiF compositions, the electrolyte was able to penetrate into the anode, indicating significant chemical interaction between the molten salt and the anode material.

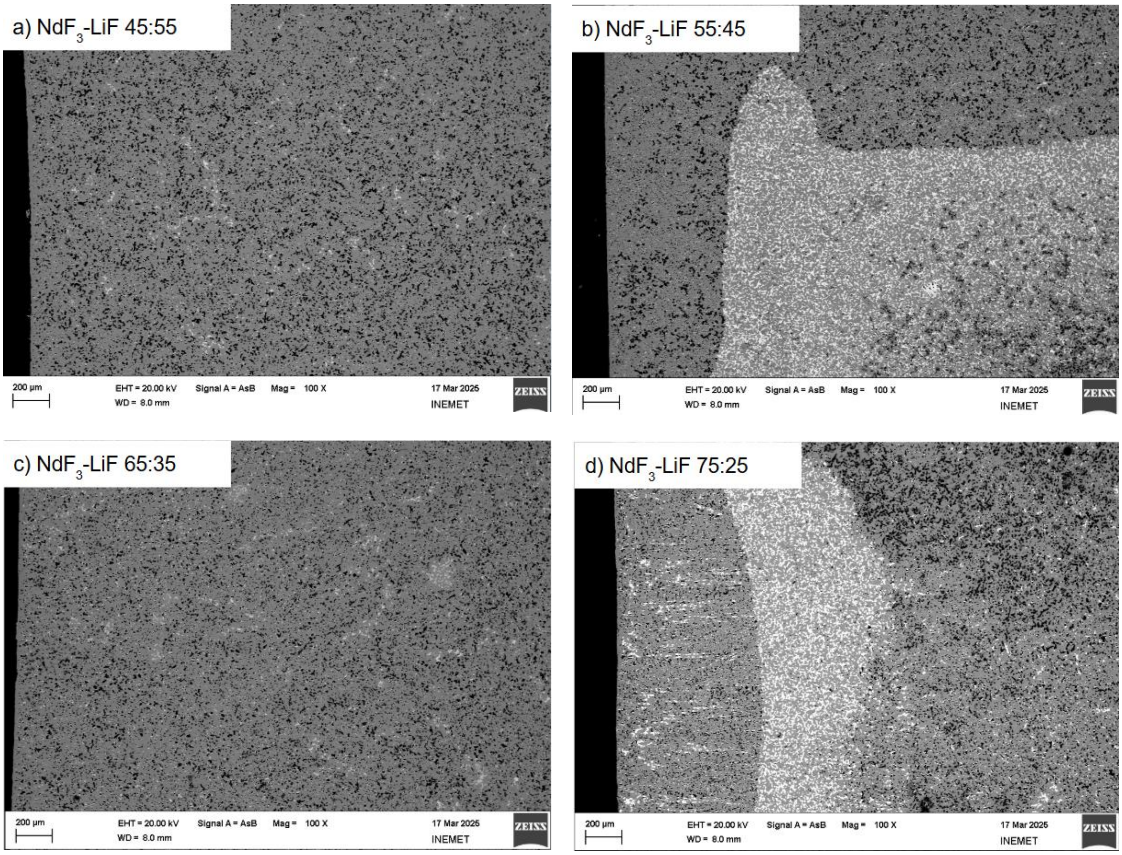

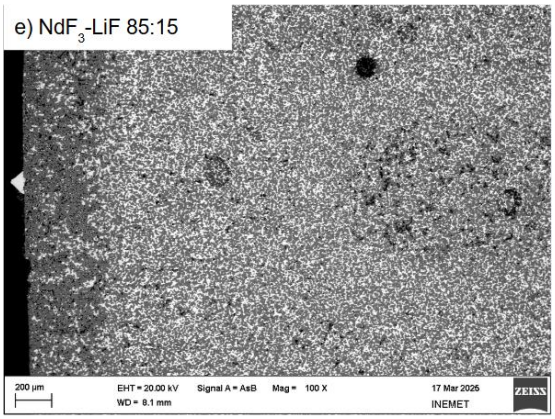

Figure 19: Top central regions of the anodes containing 20 wt% Ni after a 6 h immersion test at 1100°C, shown at 100× magnification, in NdF_3–LiF electrolytes of varying mass ration of a) 45:55, b) 55:45, c) 65:35, d) 75:25, and e) 85:15.

However, for the electrolytes with NdF_3:LiF weight ratios of 45:55 and 65:35, the SEM images revealed no clearly defined corrosion zones on the top surface of the anode. This lack of distinct zoning suggests that the anodes may not have been significantly corroded, but rather, the observed microstructure could be a result of penetration due to the high porosity of the anodes. Depending on where the samples were cut along the elongated shape of the anode, the degree of penetration might vary, leading to a more uniform microstructure across the cross-section.

In general, the anode sample showed a gradient of corrosion from the surface inward, clearly shown in Figure 19 d) 75:25 wt% of NdF_3–LiF. The outermost layer (Zone 1) was the most affected, with a dark, layered appearance and possible microcracks. This layer, in direct contact with the electrolyte and carbon crucible, underwent oxide dissolution and reduction, leading to structural degradation. The middle zone (Zone 2) was brighter and denser, indicating a transition region with partial reaction. The innermost area (Zone 3), however, contained no original $NiFe_2O_4$ structure—only NiFe alloy remained. This suggests that the electrolyte penetrated deeply into the anode and that any residual oxygen, most of which had already been removed during sintering, was likely consumed during the immersion test, potentially forming neodymium oxyfluoride (NdOF). This progression shows a clear trend of corrosion, with the outer layer heavily affected, the middle layer partially reacted, and the inner region chemically transformed into metallic alloy and oxyfluoride phases.

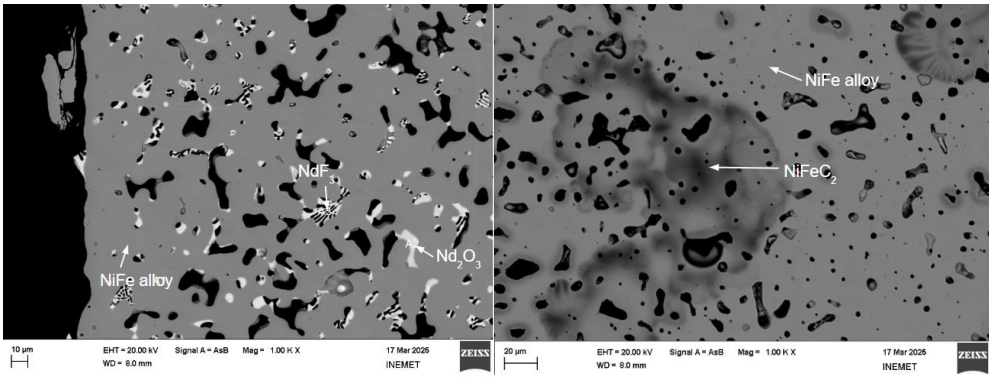

Figure 20: Anode after 6 h immersion test in NdF_3:LiF (45:55 wt%) electrolyte, at 1000× magnification: a) Top-middle section, b) Bottom-middle section.

As seen in Figure 20a, the top side of the immersed anode showed no clear signs of corrosion or formation of new phases. In contrast, the bottom side (Figure 20 b) displayed a darker gray region, indicating the formation of a NiFeC phase. This suggests that the observed carbon most likely originated from the organic binder used during the conventional sintering process. Since the image shows a cross-sectional cut, carbon diffusion from the carbon crucible can be ruled out. Additionally, the presence of carbon could also be attributed to contamination introduced during sample polishing, such as from diamond paste.

ICP-OES result

The powder electrolytes were analyzed using ICP-OES to quantify the concentrations of Li, Nd, Ni, and Fe in the electrolyte after 6 h immersion test.

Table 8: ICP-OES analysis of the electrolyte composition after 6 h immersion tests with varying NdF_3–LiF composition

No	NdF_3-LiF composition	Initial Li %	Measured Li %	Initial Nd%	Measured Nd %	Measured Ni %	Measured Fe %
1	**45:55**	14.8	14.82	32.24	4.71	<0.01	<0.01
2	**55:45**	12.11	11.79	39.4	23.24	<0.01	<0.01
3	**65:35**	9.42	9.64	46.565	9.62	<0.01	<0.01
4	**75:25**	6.73	6.8	53.73	20.35	<0.01	<0.01
5	**85:15**	4.04	4.1	60.98	35.28	<0.01	0.01

From Table 8, the Ni and Fe concentrations in the electrolyte remained very low, indicating minimal dissolution of the anode. Furthermore, the variation in NdF_3–LiF composition had little effect on the concentrations of Ni and Fe detected, suggesting that

the electrolyte composition did not significantly influence the extent of anode dissolution under the tested conditions.

XRD result

For XRD analysis, the phases present in the electrolyte were identified to understand the chemical changes occurring during the immersion test. The results showed that all five different NdF_3-LiF composition electrolytes contained three common phases: LiF, NdF_3, and $NdO_{0.67}F_{1.66}$.

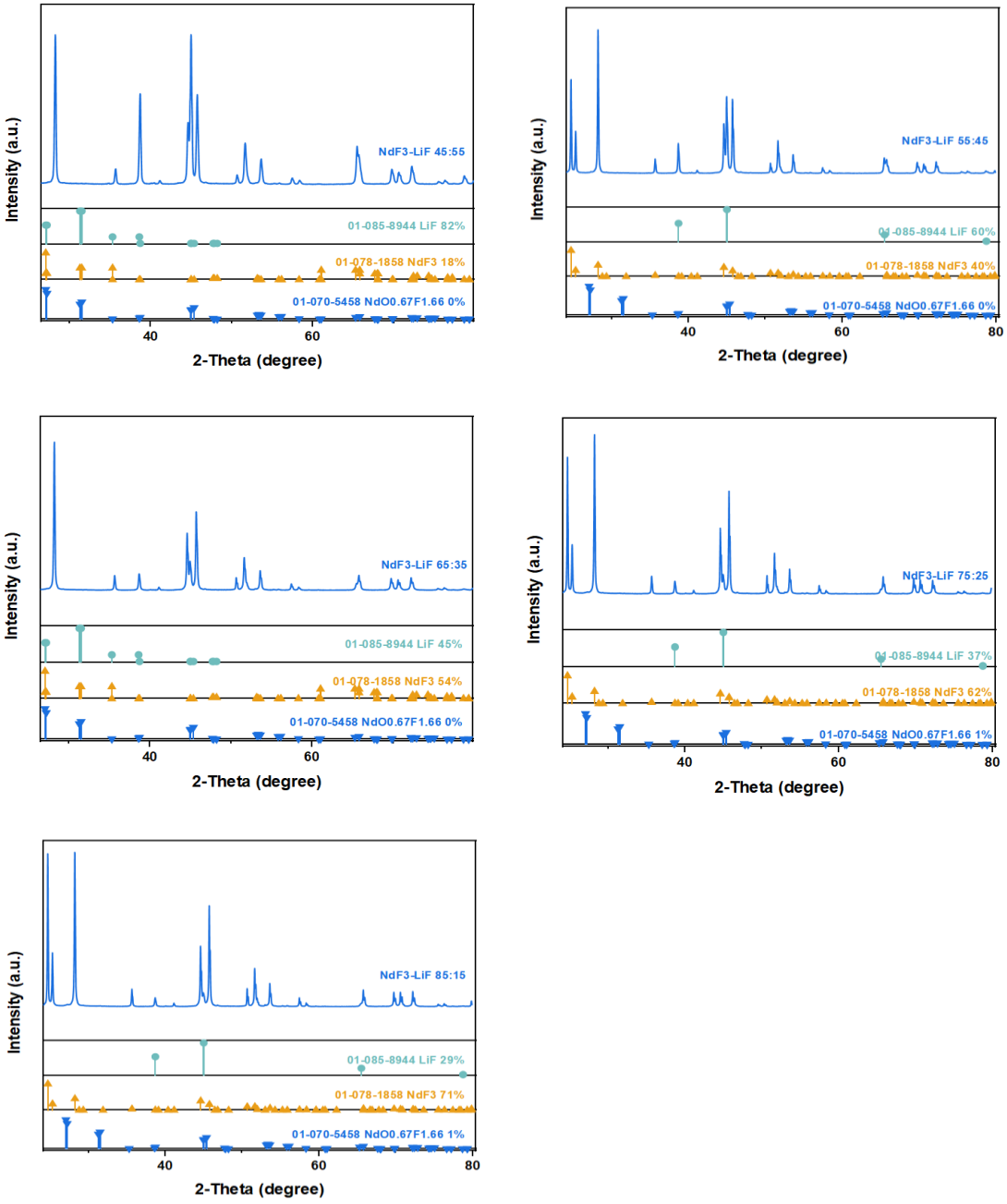

Figure 21: XRD analysis of phases in electrolytes with varying NdF_3-LiF mass ratios

The presence of the $NdO_{0.67}F_{1.66}$ phase is particularly noteworthy. Since no Nd_2O_3 was added to the system, the formation of this phase indicates a chemical reaction between NdF_3 and oxygen from the anode material. The amount of neodymium oxyfluoride detected was relatively low (approximately 0–1%), supporting the interpretation that only a small fraction of the electrolyte reacted with the anode-derived oxygen.

4.1.5 Effect of Nd_2O_3 addition

In this section, the effect of Nd_2O_3 addition on the corrosion behavior of the anode was investigated at a constant electrolyte composition of 85:15 wt% NdF_3:LiF. A conventionally sintered anode with the composition 80(85$NiFe_2O_4$–15NiO)–20Ni (wt%) was used for all experiments. Five different oxide dosages were tested: 0%, 0.5%, 1%, 1.5%, and 2% Nd_2O_3. The objective was to evaluate how varying Nd_2O_3 concentrations influence the chemical stability and corrosion resistance of the anode in the molten fluoride environment.

SEM/EDX result

The SEM images in Figure 22 show the central top regions of the anodes after immersion tests with different Nd_2O_3 additions. When no Nd_2O_3 or just 0.5% was added, only a few areas where electrolyte penetrated on the surface, indicating limited electrolyte interaction. However, as the Nd_2O_3 content increased, especially at 2%, a much more noticeable white phase spread across the anode surface. This bright grey phase is NdOF as it was confirmed through spot EDX analysis in Figure 23, where the presence of both Nd and F increased with higher Nd_2O_3 content.

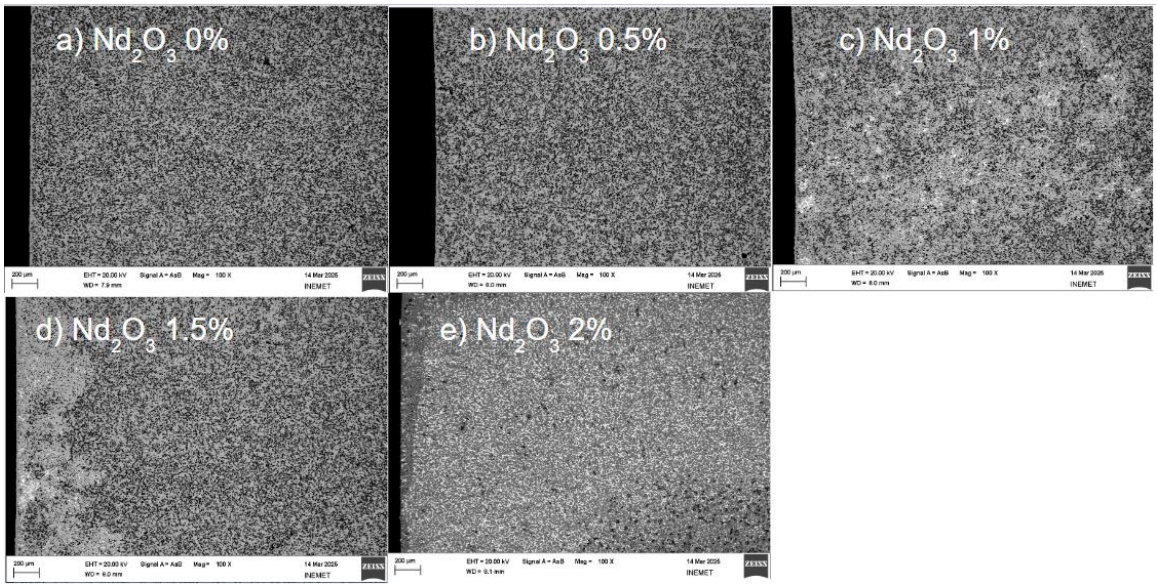

Figure 22: SEM micrographs of the inert anodes after immersion in the electrolyte with various Nd_2O_3 additions, taken at 100× magnification a) 0 wt%, b) 0.5 wt%, c) 1 wt%, d) 1.5 wt%, e) 2 wt%.

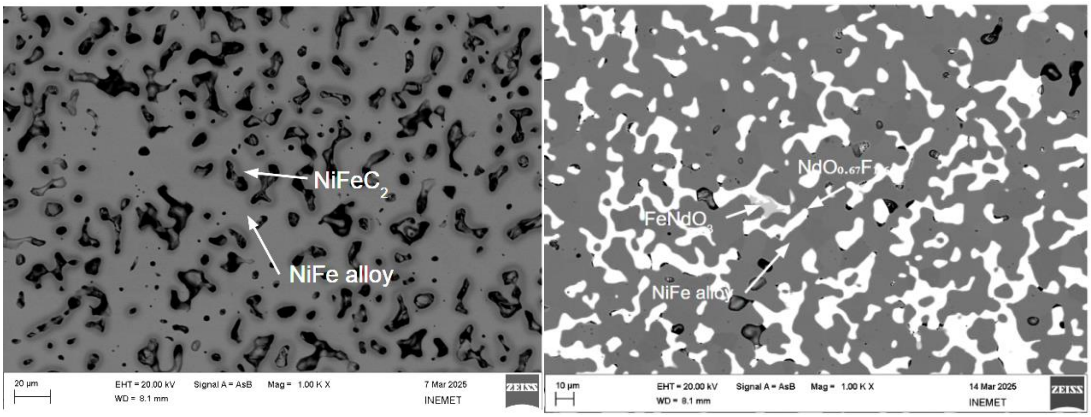

Figure 23: Spot EDX analysis of the anodes after a 6-hour immersion test at 1100°C at 100x magnification. Electrolyte composition: NdF_3-LiF 85:15 wt%, addition of Nd_2O_3 a) 0.5 wt%, b) 2 wt%

Elemental maps along the red lines showed Figure 24 that Ni, Fe, Nd, F, and O were evenly distributed, which means the electrolyte penetrated throughout the anode. Interestingly, C was also detected, which wasn't found in the SPS-made anodes. The initially high carbon signal is attributed to the embedding resin used to fix the sample in the solid matrix. Additionally, the uniformly distributed minor C peaks are likely due to residual polyvinyl alcohol (PVA) binder used during the anode sintering process.

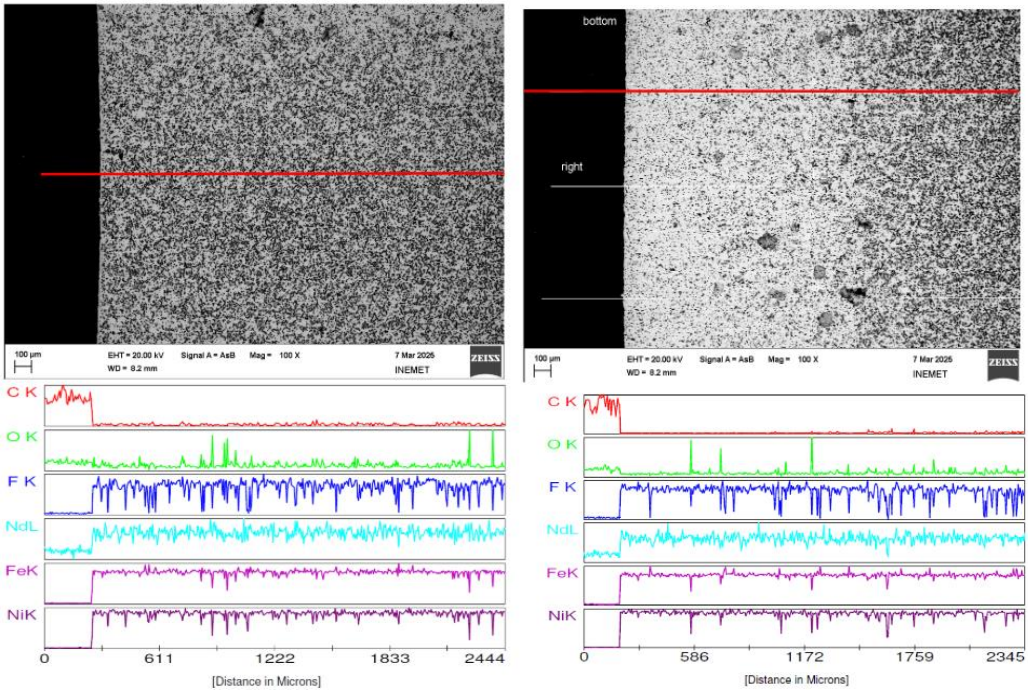

Figure 24: SEM and EDX scan of the anode corroded in the electrolyte containing the 0.5% Nd_2O_3 at 100× magnification. a) Top surface and b) right surface.

ICP-OES result

ICP-OES was conducted to assess the changes in electrolyte composition after 6 h immersion tests, results shown in Ni concentrations remained below 0.01 wt% in all cases, suggesting negligible dissolution of Ni into the electrolyte. Fe concentrations were also low and showed no meaningful variation with Nd_2O_3 addition, indicating that the corrosion of the anodes remained minimal across all tested compositions.

Table 9. Ni concentrations remained below 0.01 wt% in all cases, suggesting negligible dissolution of Ni into the electrolyte. Fe concentrations were also low and showed no meaningful variation with Nd_2O_3 addition, indicating that the corrosion of the anodes remained minimal across all tested compositions.

Table 9: ICP-OES analysis of electrolyte composition after 6 h immersion tests with varying Nd_2O_3 addition

No	Nd_2O_3 addition	Initial Li %	Measured Li %	Initial Nd%	Measured Nd %	Measured Ni %	Measured Fe %
1	0%	3.96	4.08	61.39	35.09	<0.01	0.01
2	0.50%	4.02	3.95	61.767	32.46	<0.01	0.01
3	1%	3.99	3.89	61.14	44.16	<0.01	0.01
4	1.50%	3.97	4.26	61.265	24.78	<0.01	0.01
5	2%	3.96	3.95	61.39	36.27	<0.01	0.03

XRD result

XRD results confirmed the consistent formation of LiF, NdF_3, and $NdO_{0.67}F_{1.66}$ phases in all electrolyte samples. The relative intensity of the $NdO_{0.67}F_{1.66}$ phase increased progressively with higher Nd_2O_3 additions, estimated at approximately 0%, 2%, 3%, 5%, and 6% for the 0%, 0.5%, 1%, 1.5%, and 2 wt% Nd_2O_3 additions, respectively. This trend suggests that Nd_2O_3 dissolution into the fluoride melt promotes the formation of oxyfluoride species, contributing to the evolving phase composition of the system.

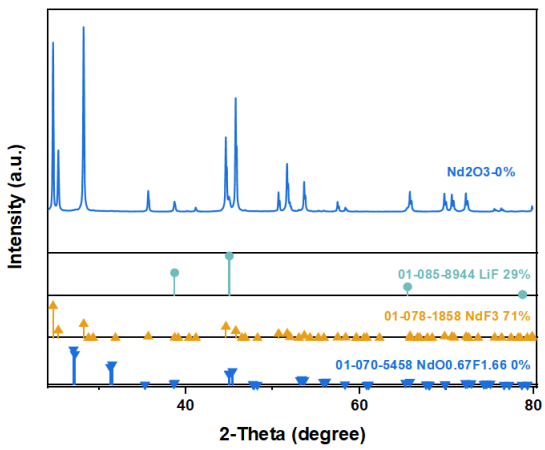

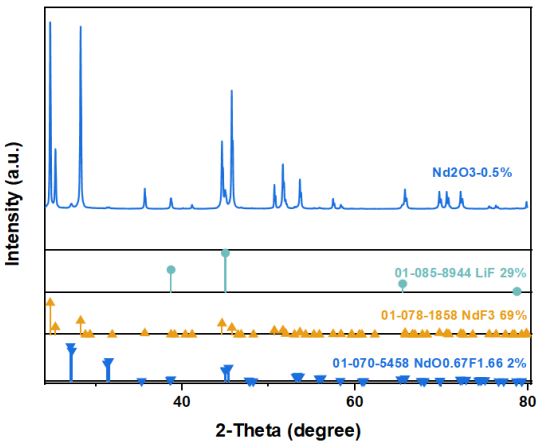

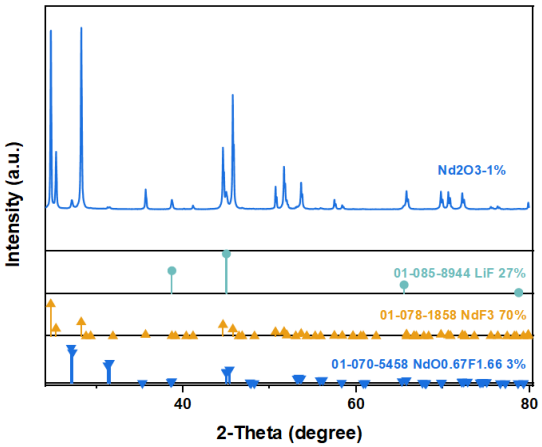

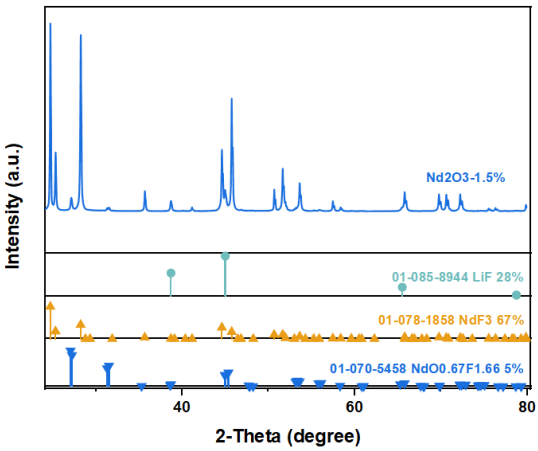

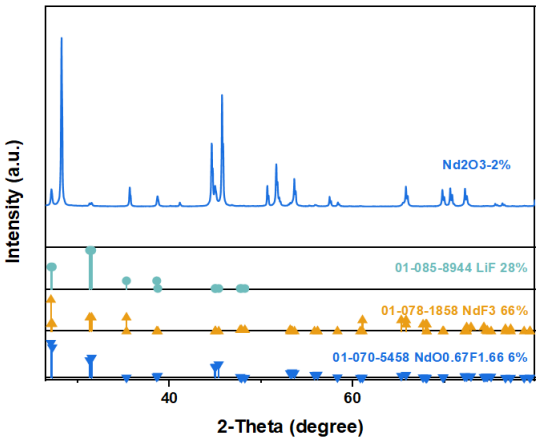

Figure 25: XRD patterns of electrolytes with different Nd_2O_3 contents.

4.2 Neodymium electrowinning

A neodymium electrowinning experiment was conducted for 2 h in an electrolyte composed of 85:15 wt% NdF_3–LiF with added 2 wt% Nd_2O_3. A conventionally sintered anode consisting of 70% ($85NiFe_2O_4$–15NiO) and 30% Ni was used.

Before initiating the electrolysis process, the melt was allowed to homogenize for approximately 30 minutes after reaching the target electrolysis temperature. This waiting period ensured that the melt composition and temperature were uniform, contributing to the consistency and reliability of the electrolysis process. Shortly after initiating the electrolysis process, an unexpected furnace shutdown occurred within the first 10 minutes. The issue was noticed immediately, and the furnace was promptly restarted. During this unplanned interruption, the temperature dropped from 1050 °C to approximately 950 °C before stabilizing again.

After molten salt electrolysis, the solidified electrolyte was difficult to remove from the graphite crucible. Therefore, the crucible had to be broken with a hammer to retrieve the electrolyte.

Figure 26: After 2 h of electrolysis a) broken graphite crucible used in the experiment; b) inert anode before electrolysis; c) post-electrolysis anode, cathode, and tungsten reference electrode.

FTIR analysis of gas evolution

FTIR spectroscopy was used to monitor gas emissions during molten salt electrolysis, revealing a continuous and progressive release of H_2O, CO_2, CO, and HF throughout the 2 h experiment. Notably, CF_4 and C_2F_6 were not detected throughout the electrolysis, suggesting that this Nd molten salt system—using a nickel ferrite-based anode—operates without producing PFCs, unlike carbon anodes.

The gradual release of H_2O likely originated from residual moisture in the electrolyte, electrodes, and other cell components. Although all materials were pre-dried, it is possible to have residual moisture. Additional moisture could have been introduced during cell assembly. Moreover, although high-purity (6.0) Ar gas was used to maintain an inert atmosphere, it contained trace amounts of moisture and oxygen. At elevated temperatures, these traces gradually desorbed and were detected as water vapor.

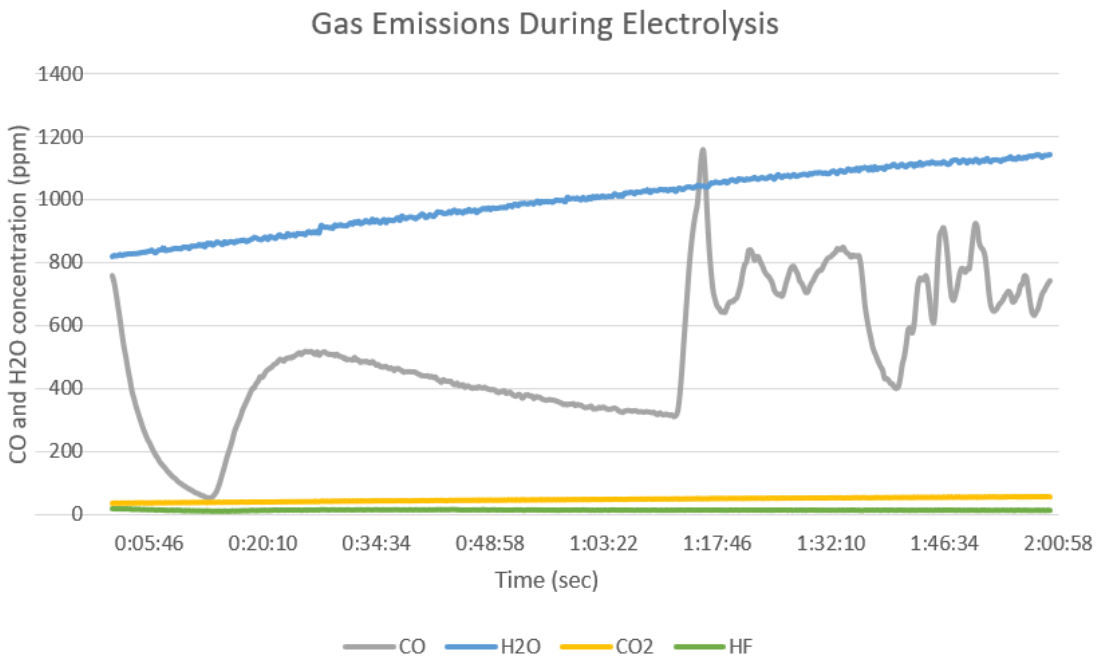

Figure 27: FTIR analysis of gas emissions (H_2O, CO_2, CO, HF) during 2 h molten salt electrolysis using a nickel ferrite-based inert anode.

The presence of CO and CO_2 is attributed to the oxidation of the carbon crucible and graphite insulation. In the electrochemically active, high-temperature environment, C readily reacts with available oxidizing agents. Trace oxygen in the system—either from the Ar gas or generated anodically—can lead to full or partial oxidation, shown in Reaction (20)-(21).

$$C + O_2 \rightarrow CO_2 \quad (20)$$

$$\mathrm{C} + \frac{1}{2}\mathrm{O_2} \rightarrow \mathrm{CO} \quad (21)$$

These reactions explain the simultaneous and increasing presence of both CO and CO_2. As shown in Figure 27, CO_2 exhibited a relatively stable and gradually increasing trend, indicating ongoing surface oxidation of the carbon crucible. In contrast, the CO signal showed irregular behavior, with multiple jumps and drops throughout the experiment. This instability suggests that the system was not in a fully stable state and that local fluctuations in O availability, temperature, or reaction pathways likely influenced the oxidation process.

HF emissions, detected in the range of 10–20 ppm, are due to moisture-induced hydrolysis of fluoride salts, generating HF in Reaction (22).

$$\mathrm{H_2O} + \mathrm{MF_n} \rightarrow \mathrm{HF} + \mathrm{M(OH)_{n-1}F} \quad (22)$$

HF formation is thermally activated, and interestingly, during an unplanned furnace shutdown within the first 10 minutes, both CO and HF signals dropped sharply. Although HF is usually detected above 850 °C and CO even earlier, the observed drop during the temperature decrease from 1050 °C to 950 °C suggests that higher temperatures significantly accelerate the reaction rates and gas release.

In summary, the observed gas emissions are strongly linked to trace moisture and oxygen contamination, along with the use of a carbon crucible under oxidative and high-temperature conditions.

Cell voltage and temperature over time

In parallel with electrochemical measurements, temperature data were acquired using an ALMEMO data acquisition system, which enabled high-resolution, time-synchronized logging from multiple thermocouples embedded in the setup.

Although the furnace was set to maintain the molten salt at 1100 °C, the thermocouple located approximately 5 cm above the electrolyte consistently measured a slightly lower temperature of around 1070 °C. The thermocouple was initially immersed in the melt but

was later lifted to prevent dissolution of its steel sheath in the corrosive environment. Due to the limited availability of materials capable of withstanding the aggressive conditions of molten salt at high temperatures, this adjustment was made to ensure the thermocouple's longevity. Throughout the electrowinning process, both the overall cell voltage and the cathode potential (measured against a tungsten reference electrode) were recorded in real time.

Figure 28: (a) Lid and internal cell temperatures measured during electrolysis. (b) Cell voltage and cathode potential vs. tungsten reference electrode over time

As illustrated in Figure 28, the cell voltage remained relatively steady for the experiment, showing a gradual rise and eventually peaking at 2.474 V near the end. A brief disturbance occurred between 0:05 and 0:15 hours, corresponding to a sudden furnace shutdown followed by an immediate restart. This incident caused a sharp but short-lived drop in both the cell voltage and cathode potential.

The increased fluctuations in cell voltage and the gradual downward shift in cathode potential were observed after approximately 1:10 hours. First, the continued deposition of Nd likely led to a local depletion of Nd^{3+} ions near the cathode surface. As the supply of reducible ions became limited, a higher overpotential was required to drive the reduction reaction. This phenomenon is consistent with classical electrochemical theory, where a lower concentration of active species at the electrode interface increases the potential needed for electron transfer [48]. Another possible reason for the higher overpotential required for Nd deposition is that Ni and Fe, which have higher melting points (above 1450°C), are deposited first at a lower potential and remain solid on the cathode surface. In contrast, Nd, which remains liquid at the electrolysis temperature, could face difficulties in deposition due to the solid Ni and Fe blocking the cathode surface. This could explain the increased overpotential observed for Nd reduction.

On the other hand, unwanted materials may have built up on the surface of the electrodes during the experiment. These could include small amounts of impurities coming from the crucible or the anode. This kind of surface contamination can interfere with the normal flow of electrons, making the electrochemical reactions slower and less efficient. As a result, the cell needs to apply more energy to keep the reactions going, which increases the overall resistance at the electrode surface [49].

Even with these effects, the cell continued to operate within the typical range needed for successful Nd deposition. The observed fluctuations in voltage and cathode potential likely reflect natural changes in the electrolyte composition and physical properties over time. One contributing factor could be the gradual evaporation of LiF, which is more volatile at high temperatures. This evaporation reduces the LiF concentration, which not only increases the melting point of the electrolyte but also raises its viscosity and electrical resistance. As a result, ion mobility is reduced, making ion transfer more difficult and potentially decreasing current efficiency [50].

SEM/EDX result

SEM images were taken from cross-sectional cuts of the anode, which had the shape of an elongated square-based prism. The SEM images reveal significant microstructural

transformation on the anode surface, as shown in Figure 29. From top to bottom, where the anode was immersed, and across different lateral sections (labeled in the figures as bottom**,** left mid**,** right low**,** and left low), a clear evolution in texture, porosity, and phase distribution was observed. The first column of images shows different sections of the anode at 100x magnification, while the second column provides a closer view at 500x magnification, with areas of interest highlighted by red circles.

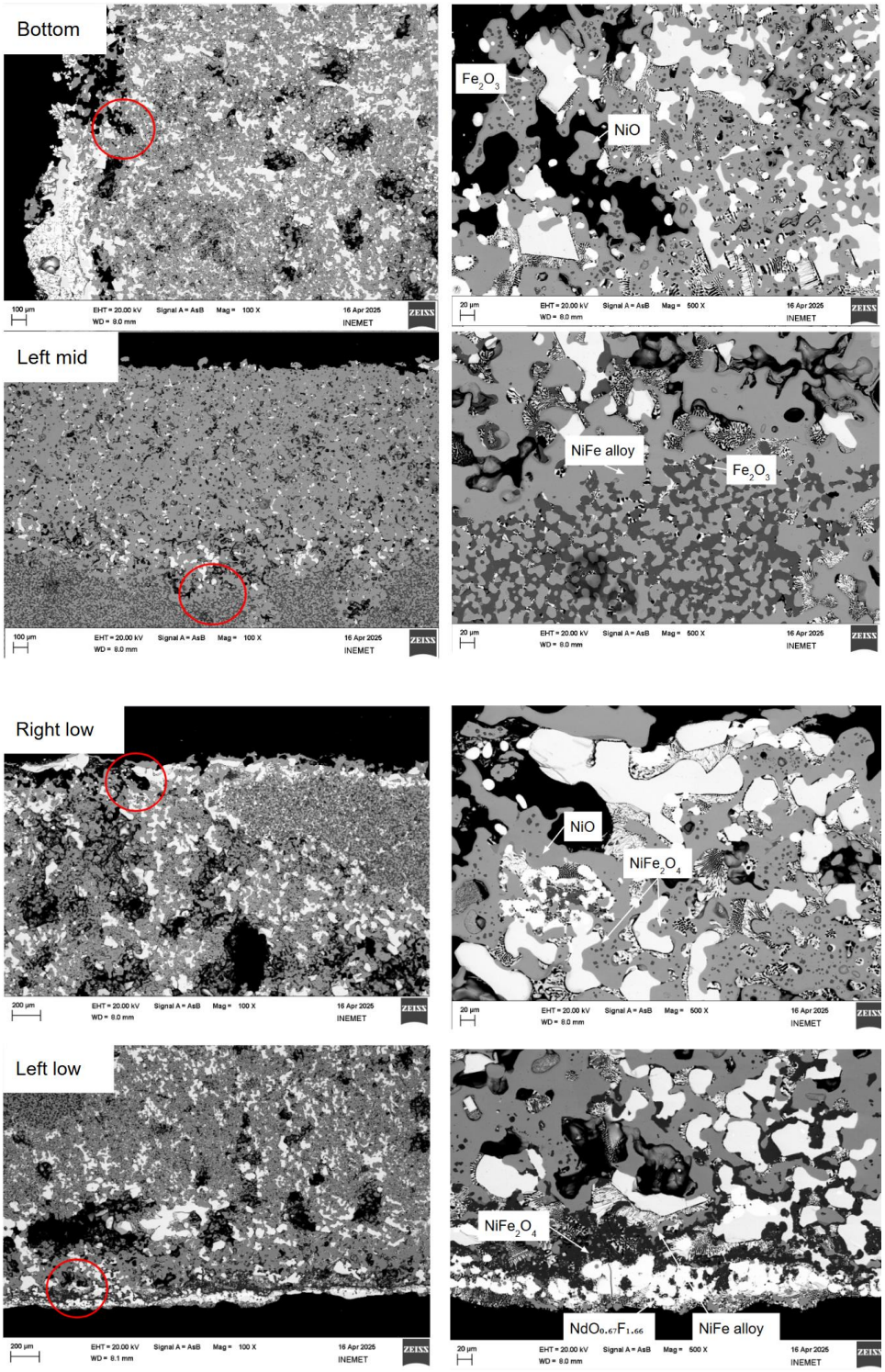

Figure 29: SEM images showing microstructural changes on the anode surface across different sections after 2 h electrolysis at 100x and 500x magnification.

In the bottom region of the anode, which was immersed in the electrolyte, surface roughening and the formation of porous zones were observed. This suggests active interaction with the molten electrolyte, likely due to oxidation reactions, as the anode material is almost fully metallic. The dissolution of the anode likely occurs via the oxidation of Ni^0 to Ni^{2+} when the applied potential drives the process. In the middle and lower regions of the anode, a $NiFe_2O_4$ phase was observed dispersed within the metallic alloy matrix. This suggests that $NiFe_2O_4$ was likely formed during the electrolysis, as it was not present in the initial anode material.

Separate NiO and Fe_2O_3 phases were found, especially near the outer edge of the anode. This suggests that the Ni and Fe from the metallic alloy were oxidized due to the continuous O_2 production on the anode during the electrolysis process.

Neodymium electrodeposition after 2 h of electrowinning

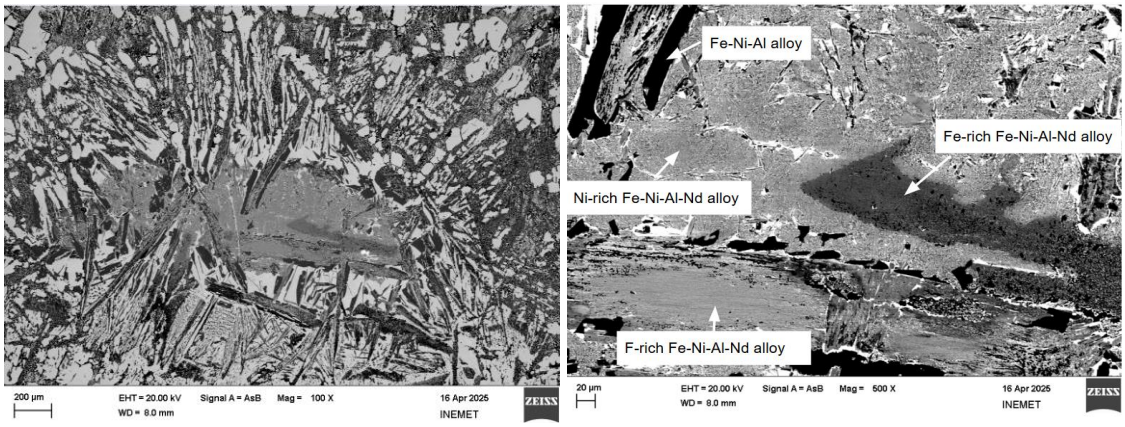

Figure 30: Neodymium metal after 2 h of electrowinning with the inert anode. a) Overview of the deposited Nd metal at 100× magnification. b) phase identification of the deposited Nd at 500× magnification.

Figure 30a shows the deposited Nd metal, with approximate dimensions of 1178 µm in width and 590.5 µm in height. From the EDX data, the purity of Nd was found to be 36.5%. As shown in Figure 30b, the elemental analysis was measured after magnifying the sample 500x. The deposit is surrounded by a Fe–Ni–Al alloy or a Fe-rich Fe–Ni–Al–Nd alloy, which appears darker in contrast and exhibits laminar grain growth.

On the outer side of this metallic alloy layer, electrolyte residues were observed, containing $NdO_{0.67}F_{1.66}$ and NdF_3 phases. The metallic alloy also contains a notable amount of Al, which likely originates from cross-contamination. This could be due to

ceramic wool used to insulate the crucible from the steel cell, which may have entered the electrolyte. Additionally, Al-containing chemicals may have entered during the drying process, as other samples are dried in the same oven.

ICP-OES result

After 2 h molten salt electrolysis, the concentrations of Li, Nd, Ni, and Fe in the solidified NdF_3–LiF electrolyte were measured using ICP-OES.

Table 10: ICP-OES result of electrolyte after 2 h of electrolysis

No	Initial Li %	Measured Li %	Initial Nd%	Measured Nd %	Measured Ni %	Measured Fe %
Electrolyte	3.96	4.2	61.39	57.84	0.01	0.06

After 2 h molten salt electrolysis, the concentrations of Li, Nd, Ni, and Fe in the solidified NdF_3–LiF electrolyte were measured using ICP-OES.

Table 10, the concentrations of Li and Nd in the electrolyte remained close to their original values after the electrolysis. The amount of dissolved Fe was slightly higher compared to previous tests, indicating that Fe is more prone to corrosion under these conditions. This increased dissolution of Fe suggests that when the inert anode dissolves in the electrolyte, the dissolved Ni and Fe would migrate toward the cathode, where they get reduced. Consequently, any dissolved Fe and Ni would be incorporated into the deposited Nd, forming an alloy. This is consistent with the fact that Fe and Ni are more noble than Nd, meaning they are reduced first at the cathode, while Nd is reduced only afterward.

However, Fe has multiple oxidation states, which allows it to undergo both reduction and oxidation during electrolysis. Specifically, Fe^{2+} can be oxidized to Fe^{3+} at the anode, and Fe^{3+} can be reduced to Fe^{2+} at the cathode. This continuous cycling of Fe between its oxidation states consumes electricity without directly contributing to the deposition of Nd. As a result, this side reaction can lower the current efficiency of the electrolysis process.

While it would have been beneficial to calculate the current efficiency, this was not possible due to the difficulty in accurately measuring the deposited Nd mass. The deposited Nd adhered to the molten electrolyte, making it impossible to isolate and measure the exact amount of Nd that was deposited on the cathode. As a result, calculating the current efficiency based on the deposited Nd mass was not feasible in

this experiment. Addressing these challenges, such as optimizing the electrode design or finding methods to better separate deposited Nd from the electrolyte, would be essential for future investigations into current efficiency.

Despite challenges such as the difficulty in removing the solidified electrolyte from the graphite crucible, significant Nd deposition occurred, with minimal dissolution of Ni and Fe into the electrolyte. SEM analysis revealed surface corrosion on the anode, with changes in microstructure indicative of interaction with the electrolyte. Gas emissions mainly consisted of H_2O, CO_2, CO, and HF, with no PFCs detected, suggesting a cleaner process compared to traditional carbon anodes.

5. Conclusion

This study explored the performance of nickel ferrite-based inert anodes in molten NdF_3–LiF electrolytes for Nd electrowinning, with a focus on corrosion behavior, electrochemical stability, and material interactions under varying experimental conditions.

Although boron nitride (BN) crucibles provided excellent chemical stability for immersion testing, their fragility and single-use limitations makes them impractical for further investigations. Graphite crucibles, on the other hand, offered a more balanced approach—combining chemical resistance with reusability and cost-efficiency—and were therefore chosen for subsequent experiments.

The corrosion resistance of $NiFe_2O_4$-based anodes was found to be highly dependent on SPS parameters. Anodes sintered at higher temperatures, particularly at 1050 °C for 10 minutes, displayed enhanced densification, which significantly reduced electrolyte infiltration. Microstructural and compositional analyses revealed a gradual degradation of $NiFe_2O_4$ into Ni-rich metallic regions and neodymium-containing oxyfluorides, indicating the progression of corrosion. This transformation was more prominent in anodes sintered at lower temperatures. Supporting this, ICP-OES measurements revealed a higher dissolution rate for Fe compared to Ni; however, due to incomplete dissolution of solid residues in the leaching solution, these values should be interpreted with caution. XRD analysis of post-test residues detected only neodymium corrosion products, suggesting that Ni and Fe either precipitated within the anode or remained in metallic form. These results underscore the importance of optimizing sintering conditions

to enhance anode longevity and chemical resistance in aggressive molten salt environments.

Conventionally sintered anodes with varying Ni content (10–50 wt%) showed minimal differences in corrosion resistance after immersion in NdF_3–LiF–Nd_2O_3 electrolytes. Only the 20 wt% Ni sample exhibited noticeable electrolyte penetration, likely due to higher porosity at its core, while other samples remained largely intact. Minimal metal dissolution and the absence of new corrosion-related phases, as confirmed by ICP-OES and XRD, suggested that porosity had a more significant impact on corrosion behavior than Ni content alone.

The NdF_3–LiF composition also played a key role in corrosion behavior. While all electrolyte formulations led to some degree of anode penetration, higher NdF_3 mass ratios (e.g., 75:25) triggered more aggressive attack, resulting in a distinct corrosion gradient and full transformation of the anode core into NiFe alloy. In this case, there was no addition of Nd_2O_3, then XRD revealed the formation of $NdO_{0.67}F_{1.66}$, suggesting that oxygen released from the oxide-based anode reacted with excess NdF_3. Despite limited Ni and Fe dissolution, the structural changes in the anode became more severe as NdF_3 content increased, highlighting the electrolyte's role in accelerating corrosion and influencing microstructural evolution.

A 2 h electrowinning test was conducted under high-temperature molten salt conditions to assess the performance of the nickel ferrite-based inert anode. However, this relatively short duration did not allow the system to reach steady-state operation, as literature suggests that at least 48 hours of continuous electrolysis are typically required for stabilization. The purity of the deposited Nd was relatively low (36.5%), indicating that further optimization of process parameters and electrode design is needed to improve product quality. Despite partial decomposition and visible interaction with the Nd-containing electrolyte, the anode remained structurally stable throughout the test. A dense Nd deposit formed at the cathode, surrounded by alloy phases containing Fe, Ni, and Al. ICP-OES confirmed low levels of metal dissolution. FTIR analysis detected gas emissions, including CO, CO_2, HF, and H_2O, primarily originating from crucible oxidation and moisture in the system. Importantly, no PFCs were detected, underscoring the environmental advantages of using inert anodes over traditional carbon-based systems.

Although current efficiency was not directly measured, the observed performance suggests that further process optimization is required to improve product purity and overall efficiency. The presence of side reactions involving dissolved Fe and Ni species,

which may undergo repeated redox cycling in the melt, could hinder overall performance. To mitigate this, pre-oxidation of the anode surface before electrolysis may reduce metal dissolution.

In summary, nickel ferrite-based inert anodes show strong potential for Nd electrowinning applications. They offer excellent corrosion resistance, high electrochemical stability, and minimal environmental impact. These findings mark an encouraging step toward greener and more efficient REE recovery. Nevertheless, to realize their full industrial potential, further work is needed—particularly in optimizing sintering conditions, minimizing porosity, and assessing long-term durability under operating conditions.

References

[1] Treatise on Geochemistry. Elsevier; 2003.

[2] Gutfleisch O, Willard MA, Brück E, Chen CH, Sankar SG, Liu JP. Magnetic materials and devices for the 21st century: stronger, lighter, and more energy efficient. Adv Mater 2011; 23(7): 821–42

[3] Ghorbani Y, Ilankoon I, Dushyantha N, Nwaila GT. Rare earth permanent magnets for the green energy transition: Bottlenecks, current developments and cleaner production solutions. Resources, Conservation and Recycling 2025; 212: 107966

[4] Hanno Vogel. Prozessoptimierung der Neodym-Schmelzflusselektrolyse zur Verringerung von Treibhausgasemissionen. Prozessoptimierung der Neodym-Schmelzflusselektrolyse zur Verringerung von TreibhausgasemissionenRWTH Aachen University 2017.

[5] Vogel H, Friedrich B. An Estimation of PFC Emission by Rare Earth Electrolysis. In: Martin O, editor. Light Metals 2018. Cham: Springer International Publishing 2018; 1507–17.

[6] Ioan Galasiu, Rodica Galasiu, Jomar Thonstad. Inert Anodes For Aluminium Electrolysis. 1st edition.

[7] C. K. Gupta N. Extractive Metallurgy of Rare Earths. CRC press 2005.

[8] Jordens A, Cheng YP, Waters KE. A review of the beneficiation of rare earth element bearing minerals. Minerals Engineering 2013; 41: 97–114

[9] statista. Mine production of rare earths worldwide in 2024, by leading country.

[10] statista. Neodymium oxide price worldwide from 2009 to 2020 with a forecast for 2021 to 2030. Available from: URL:

[11] K. Grjotheim and Halvor Kvande. Introduction to aluminium electrolysis: understanding the Hall-Hérloult process. 2nd edition. Germany: Aluminium-Verlag 1993.

[12] Wikipedia. Hall–Héroult process.

[13] Thonstad J, Rolseth S, Keller R. On the Mechanism Behind Low Voltage PFC Emissions. In: Sadler BA, editor. Light Metals 2013. Cham: Springer International Publishing 2016; 883–5.

[14] Nourse ES. The regional workshops on primary care. J Med Educ 1975; 50(12 pt 2): 201–9[15] Galasiu I, Galasiu R, Nicolescu C. Metallic Inert Anodes for Aluminium Electrolysis. In: Gaune-Escard M, Seddon KR, editors. Molten Salts and Ionic Liquids. Wiley 2010; 123–31.

[16] Windisch CF, JR., Strachan DM, Henager CH, JR., Alcorn TR, Tabereaux, A. T. & Richards, N. E. Materials characterization of cermet anodes tested in a pilot cell 1993.

[17] Olsen E, Thonstad J. Journal of Applied Electrochemistry 1999; 29(3): 293–9

[18] Padamata SK, Singh K, Haarberg GM, Saevarsdottir G. Review—Primary Production of Aluminium with Oxygen Evolving Anodes. J. Electrochem. Soc. 2023; 170(7): 73501

[19] Gibilaro M, Meyer P, Massot L, Bouvet S, Laurent V, Chamelot P. Influence of operating conditions on cermet inert anode corrosion in cryolite for aluminium production. Corrosion Science 2021; 192: 109773

[20] Nightingale SA, Longbottom RJ, Monaghan BJ. Corrosion of nickel ferrite refractory by Na3AlF6–AlF3–CaF2–Al2O3 bath. Journal of the European Ceramic Society 2013; 33(13-14): 2761–5

[21] HE H, WANG Y, LONG J, CHEN Z. Corrosion of NiFe2O4–10NiO-based cermet inert anodes for aluminium electrolysis. Transactions of Nonferrous Metals Society of China 2013; 23(12): 3816–21

[22] Abbasalizadeh A, Malfliet A, Seetharaman S, Sietsma J, Yang Y. Electrochemical Extraction of Rare Earth Metals in Molten Fluorides: Conversion of Rare Earth Oxides into Rare Earth Fluorides Using Fluoride Additives. J. Sustain. Metall. 2017; 3(3): 627–37

[23] Akolkar R. Perspective—Is Sustainable Electrowinning of Neodymium Metal Achievable? J. Electrochem. Soc. 2022; 169(4): 43501

[24] Abedi M, Sovizi S, Azarniya A*, et al.* An analytical review on Spark Plasma Sintering of metals and alloys: from processing window, phase transformation, and property perspective. Critical Reviews in Solid State and Materials Sciences 2023; 48(2): 169–214

[25] Munir ZA, Anselmi-Tamburini U, Ohyanagi M. The effect of electric field and pressure on the synthesis and consolidation of materials: A review of the spark plasma sintering method. J Mater Sci 2006; 41(3): 763–77

[26] Shing Kuai and Ji Meng. Electrolysis: Theory, Types and Application: Molten salt electrolysis for sustainable metals exraction and materials processing - A review. Nova Science Publishers 2010.

[27] Guo X. Dissolution and Electrochemical Reduction of Rare Earth Oxides in Fluoride Electrolytes. Delft University of Technology 2021.

[28] Xiaoling GUO, Jilt SIETSMA, Yongxiang YANG, editor. Solubility of rare earth oxides in molten fluorides. The Netherlands; 2014.

[29] HuXianWei. Study on Ionic Structure and Its Application of NdF3-LiF-Nd2O3 System Melts. PhD thesisNortheastern University 2009.

[30] Hu X, Wang Z, Gao B*, et al.* Research on form of Nd-F-O complex ions in NdF3-LiF-Nd2O3 melts. In: Research on form of Nd-F-O complex ions in NdF3-LiF-Nd2O3 melts; 2009. IEEE; 1–5.

[31] Stefanidaki E, Hasiotis C, Kontoyannis C. Electrodeposition of neodymium from LiF–NdF3–Nd2O3 melts. Electrochimica Acta 2001; 46(17): 2665–70

[32] Stefanidaki E, Photiadis GM, Kontoyannis CG, Vik AF, Østvold T. Oxide solubility and Raman spectra of NdF3–LiF–KF–MgF2–Nd2O3 melts. J. Chem. Soc., Dalton Trans. 2002; (11): 2302–7

[33] Thudum R, Srivastava A, Nandi S, Nagaraj A, Shekhar R. Molten salt electrolysis of neodymium: electrolyte selection and deposition mechanism. Mineral Processing and Extractive Metallurgy 2010; 119(2): 88–92

[34] Lee G-G, Jo S-K, Lee C-K, Ryu HY, Lee JH. Study On Electrolysis for Neodymium Metal Production. In: Neelameggham NR, Alam S, Oosterhof H, Jha A, Dreisinger D, Wang S, editors. Rare Metal Technology 2015. Cham: Springer International Publishing 2016; 249–52.

[35] Neelameggham NR, Alam S, Oosterhof H, Jha A, Dreisinger D, Wang S, editors. Rare Metal Technology 2015. Cham: Springer International Publishing; 2016.

[36] Sarfo P, Das A, Young C. Extraction and optimization of neodymium from molten fluoride electrolysis. Separation and Purification Technology 2021; 256: 117770

[37] Dube A, Malode SJ, Alshehri MA, Shetti NP. Electrochemical degradation of some toxic molecules- a concise review of recent studies. Journal of Environmental Chemical Engineering 2024; 12(6): 114916

[38] Olsen E, Thonstad J. The Behaviour of Nickel Ferrite Cermet Materials as Inert Anodes. In: Tomsett A, Johnson J, editors. Essential Readings in Light Metals. Cham: Springer International Publishing 2016; 1110–8.

[39] Bacon JR, Butler OT, Cairns WRL*, et al.* Atomic spectrometry update – a review of advances in environmental analysis. J. Anal. At. Spectrom. 2021; 36(1): 10–55

[40] Evans EH, Pisonero J, Smith CMM, Taylor RN. Atomic spectrometry update: review of advances in atomic spectrometry and related techniques. J. Anal. At. Spectrom. 2020; 35(5): 830–51

[41] Carter S, Fisher AS, Goodall PS, Hinds MW, Lancaster S, Shore S. Atomic spectrometry update. Industrial analysis: metals, chemicals and advanced materials. J. Anal. At. Spectrom. 2010; 25(12): 1808

[42] surfacesciencewestern. Scanning Electron Microscopy coupled with Energy Dispersive X-ray (SEM/EDX) Spectroscopy.

[43] Barbara L Dutrow, Christine M. Clark. X-ray Powder Diffraction (XRD): Louisiana State University, Eastern Michigan University.
[44] Bunaciu AA, Udriştioiu EG, Aboul-Enein HY. X-ray diffraction: instrumentation and applications. Crit Rev Anal Chem 2015; 45(4): 289–99
[45] Fathi Habashi. Handbook of Extractive Metallurgy. Wiley company 1997.
[46] Kwon Sukcheol, Lee Youngjun, Ryu Hongyeol, Lee Gogi, Cho Seonggu, Lee Jonghyun. High temperature stability of nitride ceramic materials in LiF-NdF3-Nd2O3 molten salts system. Korean. J. Mater. Res. 2015; 25(12): 694~702-694~702
[47] Oke SR, Ige OO, Falodun OE, Obadele BA, Mphahlele MR, Olubambi PA. Influence of sintering process parameters on corrosion and wear behaviour of SAF 2205 reinforced with nano-sized TiN. Materials Chemistry and Physics 2018; 206: 166–73
[48] Allen J. Bard. Electrochemical methods. USA: Wiley 2001.
[49] Zhu H. Rare Earth Metal Production by Molten Salt Electrolysis. In: Kreysa G, Ota K, Savinell RF, editors. Encyclopedia of Applied Electrochemistry. New York, NY: Springer New York 2014; 1765–72.
[50] Dominic Feldhaus, Marie-Theres Tschauner, Bernd Friedrich. Influence of LiF on the synthesis of the neodymium & praseodymium molten salt electrolysis 2021.